European Wind Energy Master

Evaluating the workability of On-Site Assembly of a 15MW Wind Turbine Blade on a Semi-Submersible Floating Wind Turbine Using a Crane Vessel

MSc Thesis

Isabelle van der Kaaij

TU Delft
NTNU
Norwegian University of Science and Technology
GustoMSC | NOV

Evaluating the workability of On-Site Assembly of a 15MW Wind Turbine Blade on a Semi-Submersible Floating Wind Turbine Using a Crane Vessel

MSc Thesis

by

Isabelle van der Kaaij

in partial fullfillment of the requirements to obtain the degree of

Master of Science in Offshore and Dredging Engineering at the Delft University of Technology
&
Master of Science in Wind Energy Technology at the Norwegian University of Science and Technology

under the **European Wind Energy Master** programme.

To be defended publicly on Friday April 28th, 2023.

Student number:	4461282	TU Delft
	557419	NTNU
Project Duration:	January, 2022 - April, 2023	
Supervisors:	Dr. ir. G. Lavidas	TU Delft
	Prof. dr. ir. Z. Gao	NTNU
	Ir. F.A. Huijs	GustoMSC

Delft University of Technology

Norwegian University of Science and Technology

Acknowledgement

Firstly, I would like to express my sincere gratitude to my university supervisors. I want to thank George Lavidas for his effort and guidance throughout the project. Additionally, your insightful questioning of my research questions and motives helped me to ensure that I was completely satisfied with my approach and direction. I also want to extend my gratitude to Zhen Gao for the enlightening discussions we had during my literature study in Trondheim. I am thankful for your unwavering support, and I appreciate how you continued showing this commitment during my period in the Netherlands.

This research project is performed under the guidance of GustoMSC. From GustoMSc, I would first of all like to thank Fons Huijs. Fons, your invaluable support and vast knowledge proved to be instrumental in guiding me through my thesis. Your sharp critical eye helped to identify areas that required further exploration, leading to insightful and engaging discussions. Our weekly meetings were always thought-provoking, leaving me with a deeper understanding of the subject matter and renewed sense of curiosity. Moreover thanks to Peter Veldman for consistently being available to provide feedback and guidance, as well as for boosting my confidence and morale. I am thankful for your positivity, constructive criticism and support. During the course of my thesis project, I had the pleasure of spending a considerable amount of time at the GustoMSC office. I am thankful to my colleagues for generously sharing their knowledge and expertise and for their willingness to assist me whenever needed.

Finally I would like to thank my family, friends and everybody that has aided and encouraged me throughout these years. First of all, thanks to Mary, Bill, and Annemarth for being my constant supporters throughout my journey from diapers to diplomas. A huge thank you to Miek, Zola, and Anouk for providing me with the much-needed encouragement and entertainment during the times when I needed it the most. And at last, a shoutout to my fellow EWEM students, who made the Scandinavian and Arctic adventures some of the most memorable experiences of my life. Thank you all, from the bottom of my heart.

It brings me great pleasure to state that this thesis signifies not only the completion of my European Wind Energy Master program, but also the conclusion of my academic journey. I have enjoyed the ride.

Isabelle van der Kaaij
Delft, April 2023

Summary

To meet the net-zero emissions targets set by the Paris Climate Agreement in 2015, a transition to renewable energy sources is essential. Offshore wind energy is poised for significant growth, with three major trends emerging: larger wind turbines, offshore wind farm sites located in deeper waters further from the coast, and a shift towards floating offshore wind energy. While current floating wind turbines are installed using a tow-to-site strategy, the increasing size of turbines and foreseen implementation scale raises the question if on-site installation will be more a viable option.

On-site installation of offshore wind turbines is weather-restricted, time-limited, and sensitive to environmental conditions. The stick-built method is often used for bottom-fixed wind turbines, with blade installation, specifically the connection between the blade root and the hub, as a critical phase. For floating-to-floating installations, wave-induced movements of both the wind turbine and vessel create additional challenges. This research investigates the operational feasibility of on-site installation of the NREL 15 MW wind turbine blade on a semi-submersible floating wind turbine, the GustoMSC Tri-floater, using a floating monohull crane vessel. The operational feasibility of the single blade installation is determined by assessing its workability.

In this research, a simplified frequency-domain multi-body model was used to determine the motion Response Amplitude Operators (RAOs) of the Tri-floater and the crane vessel, and subsequent the relative motion RAOs between the crane tip and the hub. The model assumed first order potential flow, rigid body motions for the Tri-floater and the crane vessel, and neglected wind and current loads. The motions of the Tri-floater and the crane vessel were analysed and the hydrodynamic effect of one body on the other was investigated. The response spectrum for different significant wave heights, peak periods and wave directions were computed based on the relative motion RAO and JONSWAP wave spectrum. The Most Problable Maxima were computed for different combinations of significant wave height, peak period and wave directions, and tested against the relative motion criteria. The relative motion criteria were defined as $\pm$ 1 m, $\pm$1 m and $\pm$2.5m in the x-, y-, and z-direction respectively. The workability of a floating-to-floating operation in a site with moderate wave conditions in the Gulf of Maine was then calculated, followed by a comparison with the workability of fixed-to-fixed and floating-to-fixed operations. Furthermore, the wave directionality of the workability was assessed. Finally, an overview was presented on alternative on-site solutions for blade installation involving at least one floating element.

The comparison of the multibody and single-body models revealed that positioning the crane vessel next to the Tri-floater resulted in shielding, diffraction, radiation and reflection effects. The relative surge was limiting, caused by the crane vessel roll angle. At the site, the workability for floating-to-floating operation was 31%. The computation was performed conservatively, meaning that the values corresponded to the maximum Most Probable Maxima obtained from all wave directions. A sensitivity analysis on wave direction showed that the wave direction has significant impact on the relative motion and the workability. The optimal wave orientation resulted in a floating-to-floating workability of 51%. The workability of a floating-to-fixed operation was found comparable to that of a floating-to-floating operation. The workability of a fixed-to-fixed operation was found to be 87%.

The preliminary findings confirm that the workability of on-site installation for floating-to-floating operations is significantly more challenging than that of fixed-to-fixed operations. However, the workability for floating-to-floating is comparable to that of floating-to-fixed operations.

This suggests that the workability may not be significantly impacted by the introduction of floating wind turbines, making the transition from floating-to-fixed to floating-to-floating installations less challenging. To comprehensively understand the variation in workability between floating-to-fixed and floating-to-floating installations, additional research is recommended, which should include wind loads and blade pendulum motion. Another area for further research could be the development of a specialized blade installation tool, which could accelerate successful on-site installation of floating wind turbines.

Nomenclature

Abbreviations

BIT	Blade Installation Tool
CoB	Center of Buoyancy
CoG	Center of Gravity
DNV	Det Norske Veritas
DoF	Degree of Freedom
DP	Dynamic Positioning
GM	Metacentric Height
GWEC	Global Wind Energy Council
IEA	International Energy Agency
IRENA	International Renewable Energy Agency
LCG	Longitudinal Center of Gravity
MPM	Most Probable Maximum
RAO	Response Amplitude Operator
RW	Royal Wagenborg
SWL	Still Water Level
TCG	Transverse Center of Gravity
TLP	Tension-Leg Platform
TWD	Temporary Works Design
UK	United Kingdom
USA	United States of America
VCG	Vertical Center of Gravity
WBI	Wind Blade Installation

Number sets

$\mathbb{I}$	Imaginary numbers

$\mathbb{R}$	Real numbers

Other symbols

ϵ	Phase angle
η	Free surface elevation
$\mathbf{U_b}$	Velocity of a body in motion
$\mathbf{V}$	Fluid velocity vector
ν	Kinematic viscosity
ω	Wave frequency
ϕ)	Velocity potential
ρ	Fluid density
α_{u}	Weather uncertainty factor
$\mathbf{A}$	Added mass matrix
$\mathbf{B}$	Damping matrix
$\mathbf{F}^{\mathrm{ext}}$	External force vector
$\mathbf{K}$	Structural stiffness matrix
$\mathbf{M}$	Mass matrix
$\mathbf{X}$	System motion vector
H_s	Significant wave height
k_{xx}	Radius of gyration in roll
k_{yy}	Radius of gyration in pitch
k_{zz}	Radius of gyration in yaw
m	Meter
t	Metric tonnes
T_p	Peak period
T_z	Zero-crossing period
A	Wave amplitude
g	Gravitational constant
$\mathrm{GM_L}$	Longitudinal Metacentric Height
$\mathrm{GM_T}$	Transverse Metacentric Height
H	Wave height
h	Water depth
k	Wave number

OP_{LIM}	Operational Limit
OP_{WF}	Operational Limit for Weather Window
p	Fluid pressure
T	Wave period
T_C	Contingency Time
T_{POP}	Planned Operation Period Time
T_R	Reference Time
z	Water column height

Table of Contents

List of Figures **x**

List of Tables **xii**

1 Introduction **1**

1.1 Offshore wind energy outlook 1

1.2 Floating wind energy outlook 2

1.3 Floating offshore wind turbines 3

1.4 Problem description 4

1.5 Research objective 5

1.6 Report outline 6

2 Marine operations **7**

2.1 General standards for marine operations 7

2.2 Wind turbine installation procedures 9

2.3 Single blade installation 11

3 Method and software **14**

3.1 Methodology 14

3.2 Software 17

4 Model and assumptions **18**

4.1 Unit description 18

4.2 Unit lay-out 20

4.3 Coordinate system 22

4.4 Assumptions 24

4.5 Environmental conditions 24

5 Relative motion criteria **27**

5.1 Mating criteria 27

5.2 Relative motion criteria 28

6 Results: motions and workability **31**

6.1 Natural frequencies 31

6.2 Absolute motion 31

6.3 Relative motion 35

6.4 Motion response and workability 37

7 Sensitivity study: wave direction **40**

7.1 Floating-to-floating operation 40

7.2 Floating-to-fixed operation 42

8 Alternative solution **44**

8.1 Fixed-to-fixed solutions 44

8.2 Floating-to-fixed solutions 45

9 Conclusion **48**

10 Discussion and recommendations **50**

Bibliography **52**

Appendices **55**

Appendix A: Environmental Conditions 62

Appendix B: Wave force RAOs 64

Appendix C: Relative phase 65

List of Figures

1.1 Global offshore wind energy outlook by 2050 [4]. 1
1.2 Wind turbine size and capacity outlook (Courtesy GustoMSC). 2
1.3 Water depth at wind farm project locations with respect to distance to shore [6]. . 2
1.4 Floating wind market outlook [5]. 3
1.5 Main types of floating substructures [11]. 4

2.1 Decision making for weather restricted operations [15]. 8
2.2 Different wind turbine installation methods [22]. 9
2.3 Multiple lift installation methods. 10
2.4 Single lift installation. 11
2.5 Three blade mounting orientations during single blade installation. 12
2.6 Schematic of main components during final mating phase [33]. 13

3.1 Methodology flowchart. 15

4.1 GustoMSC Tri-floater. 19
4.2 GustoMSC Ensis. 20
4.3 Different orientations for the Tri-floater and crane vessel. 21
4.4 Axis orientation of the multi-body model, with global wave directions indicated. . 23
4.5 Schematic overview of the relative translations. 23
4.6 Site location [41]. 25
4.7 Scatter diagram [41]. 26
4.8 Wave directionality [41]. 26

5.1 Position of the blade root center with respect to the center of the hub[44]. 28
5.2 Back view of the operation, compensation as a consequence of vessel roll and Tri-floater pitch. 29
5.3 Starboard side view of the operation, compensation as a consequence of vessel pitch and Tri-floater roll. 29
5.4 Top view of the operation, compensation as a consequence of vessel and Tri-floater yaw. 29

6.1 Comparison of wave forces acting on the Tri-floater in the single-body and multi-body models for heave, roll and pitch for waves at an incidence angle of 0, 90, and 180°. 32
6.2 Comparison of wave forces acting on the crane vessel in the single-body and multi-body models for heave, roll and pitch for waves at an incidence angle of 0, 90, and 180°. 34
6.3 Relative translation RAOs between crane tip and hub. 36
6.4 Relative amplitude in surge, for all H_s - T_p pairs in the scatter diagram of site. . . 37
6.5 Relative amplitude in sway, for all H_s - T_p pairs in the scatter diagram of site. . . 37
6.6 Relative amplitude in heave, for all H_s - T_p pairs in the scatter diagram of site. . . 38
6.7 Probability distribution for a floating-to-floating operation with a conservative approach. 38
6.8 Probability distribution for a fixed-to-fixed operation. 38
6.9 Relative motion for a floating-to-fixed operation. 39

7.1 The model with respect to the global wave direction. 40
7.2 Wave directionality in relative surge, sway and heave for a floating-to-floating operation. 41
7.3 Relative amplitude in sway for a wave direction of 240°. 42
7.4 Probability distribution in sway for a wave direction of 240°. 42
7.5 Wave directionality comparison between the relative motion of a floating-to-fixed (dark colors) and a floating-to-floating (lighter colors) operation. 43

8.1 Sjøhest Wind Blade Installation Solution by GustoMSC [46]. 45
8.2 Blade Installation Tool by TWD and RW [47]. 46
8.3 Blade Exchanger by Barge Master and TWD [48]. 46

9.1 Schematic overview of the relative translations. 48

List of Tables

2.1 Case studies [13]. 9

3.1 Software used throughout this research 17

4.1 IEA 15 MW wind turbine characteristics [35]. 18

4.2 Tri-Floater design characteristics for configuration with the NREL 15 MW turbine [38]. 19

4.3 Ensis design characteristics [39]. 20

4.4 Tri-Floater loading conditions. 20

4.5 Crane vessel loading conditions. 20

4.6 Global motion components. 22

4.7 Degrees of freedom for the multibody model. 23

4.8 Points of interest. 23

4.9 Environmental conditions. 25

4.10 Site parameters [41]. 25

4.11 Site coordinates [41]. 25

6.1 Natural frequencies and natural periods for the Tri-floater and the crane vessel. . . 31

Chapter 1

Introduction

1.1 Offshore wind energy outlook

To combat the rise in global temperatures and achieve the goal of limiting this rise to 1.5 °C, the Paris Climate Agreement of 2015 set a target of reaching net-zero emissions by 2050 [1]. The 26th Conference of the Parties (COP26) climate summit in Glasgow in 2021 saw several countries renewing their commitments to align with the Paris temperature goal, with over 40 countries pledging to reduce their reliance on coal-fired energy [2]. Offshore wind energy is expected to play a crucial role in reaching these targets. According to the International Renewable Energy Agency (IRENA), installation of over 2000 GW of offshore wind energy is required by 2050 [3]. Figure 1.1 illustrates the significant increase required to achieve the 1.5 ° pathway in offshore wind energy. Considering these developments, it is clear that the offshore wind energy industry is expected to grow significantly in the upcoming years.

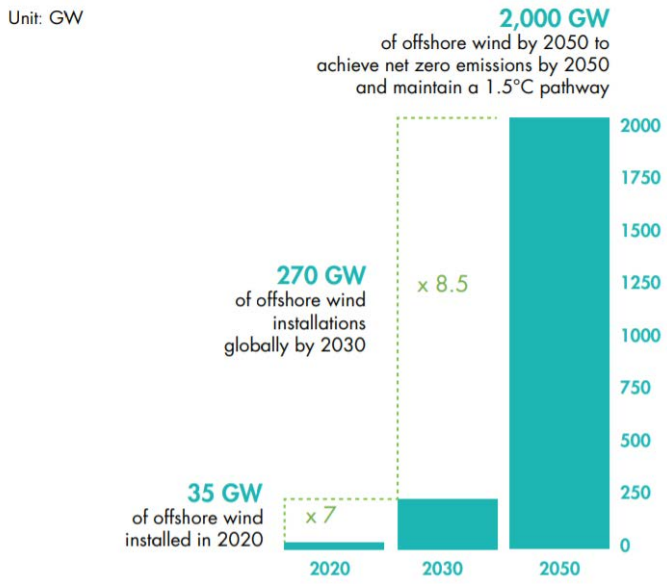

Figure 1.1: Global offshore wind energy outlook by 2050 [4].

The offshore wind energy market is witnessing a trend towards larger wind turbines, as depicted in Figure 1.2. The future is expected to bring the implementation of turbines with capacities ranging from 15 MW to 20 MW, featuring a hub height of up to 190 m and a rotor diameter of up to 250 m [5]. This trend towards larger turbines is expected to continue in the coming decades. While larger offshore wind turbines offer the potential for higher capacity factors and greater energy output, they also present new installation and maintenance challenges.

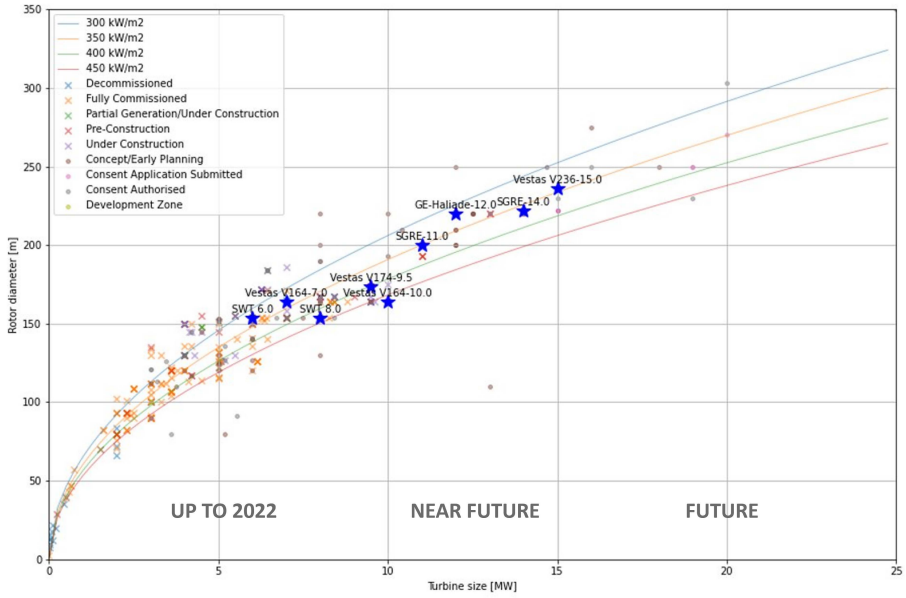

Figure 1.2: Wind turbine size and capacity outlook (Courtesy GustoMSC).

Another trend in the offshore wind industry is the move towards deeper waters and increasing distances to shores, as illustrated in Figure 1.3. This trend is expected to continue, particularly in regions where shallow water sites are limited, such as in Asia or in regions where sites close to shore are becoming scarce, such as the North Sea in Europe.

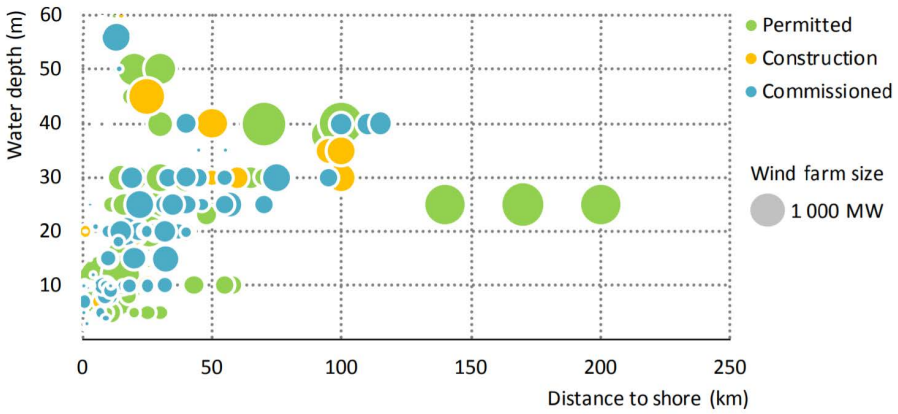

Figure 1.3: Water depth at wind farm project locations with respect to distance to shore [6].

Bottom-fixed offshore wind turbines are feasible only in water depths up to 50-60 m [7]. The cost and complexity of these foundations increase significantly with water depth. For deeper waters, alternative foundation types such as floating platforms become necessary. The Global Wind Energy Council (GWEC) predicts that bottom-fixed wind turbines will remain dominant in the offshore wind market until 2030, with floating offshore wind energy becoming commercially viable after that time [4].

1.2 Floating wind energy outlook

Floating wind energy is a rapidly emerging technology that has the potential to significantly impact the offshore wind industry. Not restricted by water depth, floating wind farms can access higher wind resources further offshore, resulting in higher capacity factors and enhanced yields. Several pilot and demonstration projects have been installed to test the feasibility of floating wind turbines

and the results have been promising. The Hywind Scotland floating array achieved a capacity factor of 54% over its first two years of operation (compared to an average of 40% for bottom-fixed offshore wind farms in the United Kingdom) and survived major storms [8].

Although the potential of floating wind energy has been demonstrated, the implementation on a large-scale is still far from being realized. As of 2022, the total global cumulative deployment of floating offshore wind turbines was only 128 MW, which is significantly less than the over 35 GW of bottom-fixed offshore wind energy [9, 3]. However, the current situation is expected to change. For instance, in 2022, Crown Estate Scotland granted leases for 17 new offshore wind projects, 10 of which utilize floating technologies [10]. The market outlook for floating offshore wind turbines is depicted in Figure 1.4. Starting from 2030, the annual growth rate in offshore wind energy is anticipated to surpass 3 GW per year, and by 2040, the rate of installation is expected to reach nearly 10 GW per year. Assuming an average turbine size of 15 MW, this would translate to around 200 turbines being installed in 2030 and approximately 670 turbines in 2040.

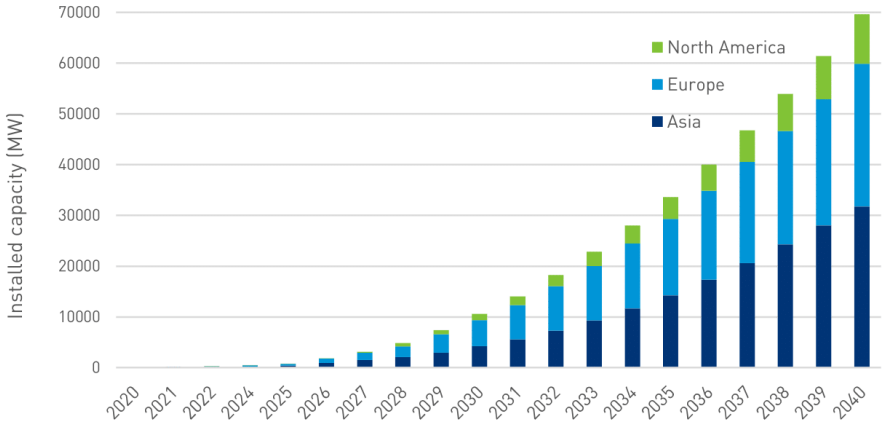

Figure 1.4: Floating wind market outlook [5].

1.3 Floating offshore wind turbines

A floating offshore wind turbine consists of the turbine itself and the substructure. The substructure consists of the floater for stability, the mooring and anchor system for maintaining position, and has a grid connection for power transmission. The majority of floating offshore wind turbines can be categorized into four substructure concepts. These concepts are distinguished by their stability mechanism, which is used to counteract the overturning moment generated by the aerodynamic thrust at the top of the turbine. Stability is achieved either through hydrostatics, moorings, or a combination of both.

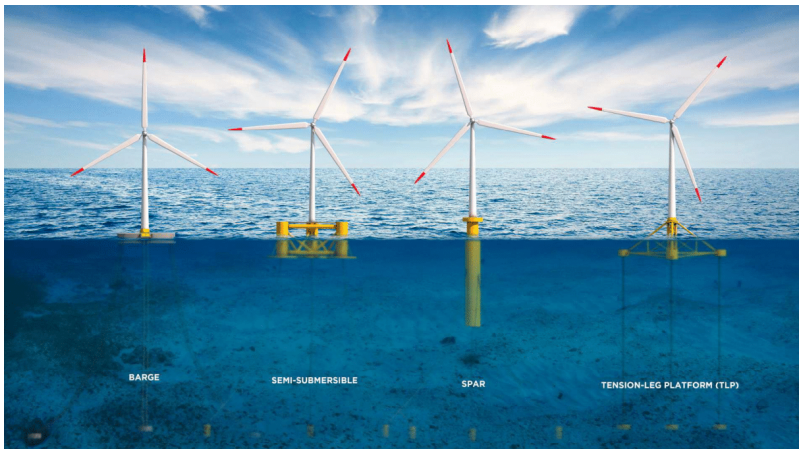

Figure 1.5: Main types of floating substructures [11].

The different concepts are visualised in figure 1.5 and described as:

- **Barges** are buoyancy-stabilized. This structure has the shallowest draft and are relatively easy to install. Increased motions are expected due to waves. More robust mooring systems and additional wave damping sources are therefore needed.
- **Semi-submersibles**, also known as semi-subs, are buoyancy-stabilised, highly versatile and can be assembled and located at various site conditions thanks to its shallow draft. Semi-subs usually consists of heave plates with three or four connected short cylinders, connected to the seabed with anchors. The relatively large waterplane inertia provides structural stiffness and relatively good hydrodynamic performance. The structure is large and complex to manufacture due to multiple welded components.
- **Spars** are ballast-stabilized. Spars are long and slender, with a center of gravity below the center of buoyancy. The technology is simple and the design is renowned for its restricted range of rotational motion. The large draft often results in installation, transportation and assembly difficulties.
- **Tension-Leg Platforms (TLPs)** are tension-stabilised by taut mooring lines anchored to the seabed. The structure experiences an excess of buoyancy forces. The shallow draft reduces the use of material and thus weight and material costs. However, the importance of mooring design and site soil conditions introduce stricter design requirements and higher operational risks.

WindEurope analysed the floating design market in 2020 and concluded that 50 floating designs were developed worldwide, of which 62% were semi-submersibles and 20% spar-buoys. Semi-submersibles are expected to dominate the floating wind industry due to their high versatility and good hydrodynamic performance.

1.4 Problem description

One of the main challenges to unlocking the immense potential of the floating wind industry is the installation of commercial-scale floating offshore wind farms of 15+ MW. Most floating wind pilot projects have used a tow-to-site strategy, which involves lifting the fully pre-assembled wind turbine onto the floater substructure at the port quayside on the port quayside followed by towing the entire floating wind turbine to its intended site. This strategy imposes several difficulties for wind farms of commercial sites. The towing distance can be large depending on port constraints for the specific foundation type, while the towing speed is restricted. Considering the large number of turbines to be towed and the fact that the towing operation itself is highly weather-sensitive, the towing operation for each individual wind turbine of a wind farm can take a considerable amount of time. Moreover as the scale of wind turbines is expected to significantly increase in the coming decades, port space is becoming an increasingly pressing issue [12]. Overall, it is doubtful whether this strategy is future-proof.

On-site installation is an alternative strategy. While it is a standard practice in bottom-fixed offshore installations, a workable and cost-effective on-site installation solution for floating wind turbines has not yet been identified. The water depth necessitates the use of a floating crane vessel, which poses significant challenges to the operation due to the wave-induced motion of both the wind turbine and the crane vessel. If these challenges can be effectively addressed, this approach may pave the way for successful on-site installation of floating wind turbines. To achieve this, it is essential to first identify and quantify the challenges accurately.

Prior to this research, a stand-alone literature review was conducted to explore current and state-of-the-art methods for bottom-fixed and floating offshore wind turbine installation [13]. Based on this review, the decision was made to investigate on-site single blade installation. The stick-built method, which installs each wind turbine component one-by-one, is preferred for its efficiency. The single blade installation is a critical aspect of this method.

The aim of this research is to investigate the operational feasibility of on-site installation of a 15 MW wind turbine blade on a semi-submersible floating wind turbine using a floating crane vessel, to analyse the factors which impact the operational feasibility and to compare it to that the on-site blade installation of bottom-fixed wind turbines. The operational feasibility is investigated by a workability assessment. A workability assessment combines the offshore environment, the motion and response of the equipment and the operational procedure into one model. The workability refers to the percentage of time during which a marine operation can be executed successfully.

1.5 Research objective

Taking into account the aim of the research and the findings from the literature study, the main research question of this study is:

What is the workability of on-site installation of a 15 MW wind turbine blade on a semi-submersible floating wind turbine using a floating crane vessel and how does it compare to the on-site blade installation of bottom-fixed wind turbines?

The following sub-questions need to be answered to find an answer to the main research question:

1. What is the workability to install a 15 MW wind turbine blade on a semi-submersible floating offshore wind turbine with a floating crane vessel?
   (a) What is the relative motion criteria of the operation?
   (b) How does the global motion response in of the multi-body model in waves compare to the motion response of the single bodies? What are different interaction phenomenons that occur?
   (c) What is the relative motion between the crane tip and the hub during the operation?
   (d) What is the workability of the floating-to-floating operation?
2. In what way is the workability of a floating-to-floating operation influenced by the wave directionality?
3. How does this workability compare to that of an on-site installation of bottom-fixed wind turbines and what can be done to align these?

1.6 Report outline

This report is structured as follows.

Chapter 2 presents a background on marine operations. Moreover current procedures for installing offshore wind turbines are described. The procedure for single blade installation is described and the critical phase of the operation is analysed.

Chapter 3 provides a detailed overview of the methodology and software used in this study.

Chapter 4 describes the input to the model, including the floating wind turbine and crane vessel characteristics, their orientation, and site selection. The chapter summarises the main assumptions and defines the axis orientation and degrees of freedom.

Chapter 5 lists the relative motion criteria used to evaluate the motion response and to determine the workability.

Chapter 6 analyses the results of the wave-induced motion of the floating wind turbine and crane vessel, considers the effect of the presence of one body on the other, and assesses the workability of the floating-to-floating operation. A comparison with the worability of a fixed-to-fixed and floating-to-floating operation is presented.

Chapter 7 investigates the impact of wave directionality on the motions and workability.

Chapter 8 explores alternative on-site blade installation solutions.

Chapter 9 summarises the research findings and draws conclusions.

Chapter 10 discusses the limitations of the research and offers recommendations for further research.

Chapter 2

Marine operations

This chapter aims to provide an introduction to the topic of offshore installation operations. Firstly, Section 2.1 presents pertinent definitions and industry standards, along with lift classifications. Section 2.2 offers backgroudn information on offshore wind turbine installation methods, followed by a detailed description of the single blade installation and its critical phase in Section 2.3.

2.1 General standards for marine operations

Offshore wind turbine installation involves various classifications and is conducted in accordance with multiple industry standards for marine operations. It is crucial to be familiar with these classifications before choosing the appropriate offshore wind turbine installation approach.

2.1.1 Weather window

According to Det Norske Veritas (DNV) a marine operation is defined as a non-routine operation of a limited defined duration related to handling of objects and/or vessels in the marine environment during temporary phases [14]. Standards DNVGL-ST-N001 and DNVGL-ST-0437 apply for marine operations for floating wind turbines. According to the standards, offshore installation operations are considered a Level A activity indicating that operations are very sensitive to environmental conditions. Marine operations can be classified as weather restricted operations or unrestricted operations. For this research only weather restricted operations of limited defined duration are considered.

For weather restricted operations, a weather window assessment is usually performed. The DNVGL-ST-N001 [15] defines the required weather window with the required operational limit $\mathrm{OP_{WF}}$:

$$OP_{WF} = \alpha_u \cdot OP_{LIM} \tag{2.1}$$

which is the operational limit $\mathrm{OP_{LIM}}$ multiplied with the forecast uncertainty factor α_u. The duration of the operation is defined by the reference time:

$$T_R = T_{POP} + T_C \tag{2.2}$$

in which the reference time ($\mathrm{T_R}$) is determined based on the planned operation period ($\mathrm{T_{POP}}$) and the estimated maximum contingency time ($\mathrm{T_C}$), the additional time which might be necessary in case of bad weather days. In order to continue with the marine operation the weather forecast must not exceed certain limits for the given reference time. Figure 2.1 illustrates the decision-making process. Sometimes a sequence of operations is executed and the operation can not be stopped in between steps. In this case, the reference time has to be sufficient to account for all individual steps.

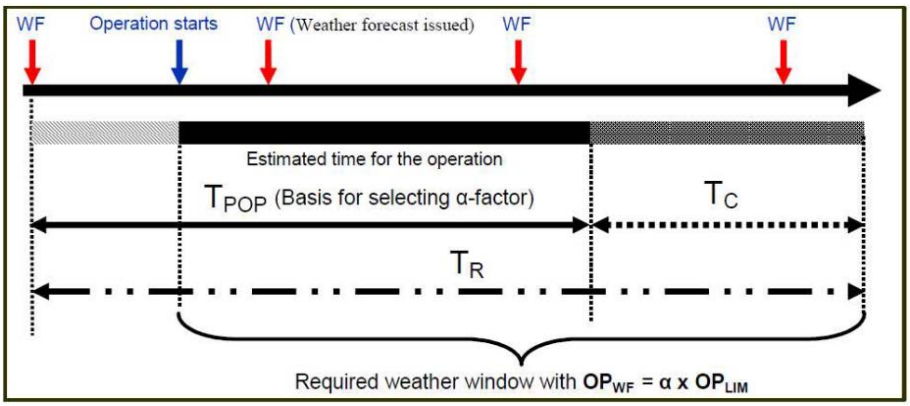

Figure 2.1: Decision making for weather restricted operations [15].

2.1.2 Lift classifications

Offshore wind turbine installation can be classified as a heavy lift operation. According to the DNVGL-ST-0378 a heavy lift is defined as *all cranes except subsea cranes with lifting capacity of 2500 kN and more* [16]. A single wind turbine lift onto a foundation classifies as a heavy lift, however. an individual blade does not. Four categories of lifting operations are distinguished depending on the type of crane support and type of structure on which the load is lifted:

1. **Fixed-to-fixed operations** are currently industry standard. An example is bottom-fixed offshore wind turbine installation with a jack-up vessel.
2. **Fixed-to-floating operations** are sometimes used in installation of floating wind demonstration projects. Examples include floating wind turbine installation with a crane at the port quayside or possibly with a jack-up in a sheltered area.
3. **Floating-to-fixed operations** are not industry standard, but several parties are researching the possibilities. Recent examples include a pre-assembled wind turbine lift from a semi-submersible crane vessel onto a bottom-fixed foundation at the Arcadis Ost 1 wind farm [17].
4. **Floating-to-floating** operations are also not widespread performed in industry, although such a lift has recently been performed with a spar floating OWT and semi-submersible vessel.

Table 2.1 illustrates the four categories of marine operations with projects that have been executed in the past. Fixed-to-fixed operations are not specified as this is common industry practice. This Table shows that there is limited experience with the other three types of lifting operations. An in-depth analysis of these case studies is provided in the literature review [13]. An example of floating-to-floating operations is the installation of the world's first floating wind farm Hywind Scotland [18]. The Hywind Scotland project adapted a sequential strategy in which the turbines were installed one after another. Upending, ballasting and mating of the turbine were performed in a sheltered area with sufficient water depth in Stord, Norway. The tower and rotor-nacelle assembly were mated onshore and a large semi-submersible crane vessel, the Saipem 7000, was used to lift the pre-assembled turbine onto the floating substructure. For this operation, a maximum significant wave height of 0.5 m and a maximum wind speed of 8 m/s were allowed [19]. After assembly, the turbine was towed to the site and connected to the mooring system.

Lifting Operation	Bottom-fixed	Semi-submersible	Spar
Fixed-to-fixed	Industry practice	N/A	N/A
Floating-to-fixed	Beatrice (2011) [20]	N/A	N/A
	FOX (2021) [17]	N/A	N/A
Fixed-to-floating	N/A	WindFloat Atlantic (2020) [9]	-
	N/A	Kincardine (2021) [21]	-
Floating-to-floating	N/A	-	Hywind Scotland (2017) [18]

Table 2.1: Case studies [13].

2.2 Wind turbine installation procedures

In this section, various installation methods for wind turbine blades and nacelles are identified. Each installation technique possesses its own set of benefits and drawbacks, which have been extensively examined in the literature review preceding this report [13]. In this section, three distinct installation methods will be explored in greater depth. These installation techniques are typically classified based on the quantity of pre-assembled components and therefore the number of lifts required for the completion of the process. Wind turbines comprise of five primary elements: the tower, which may be divided into several parts, the nacelle, and three blades. Ahn et al. [22] provide an overview of the primary offshore wind turbine installation procedures, as illustrated in Figure 2.2 [22].

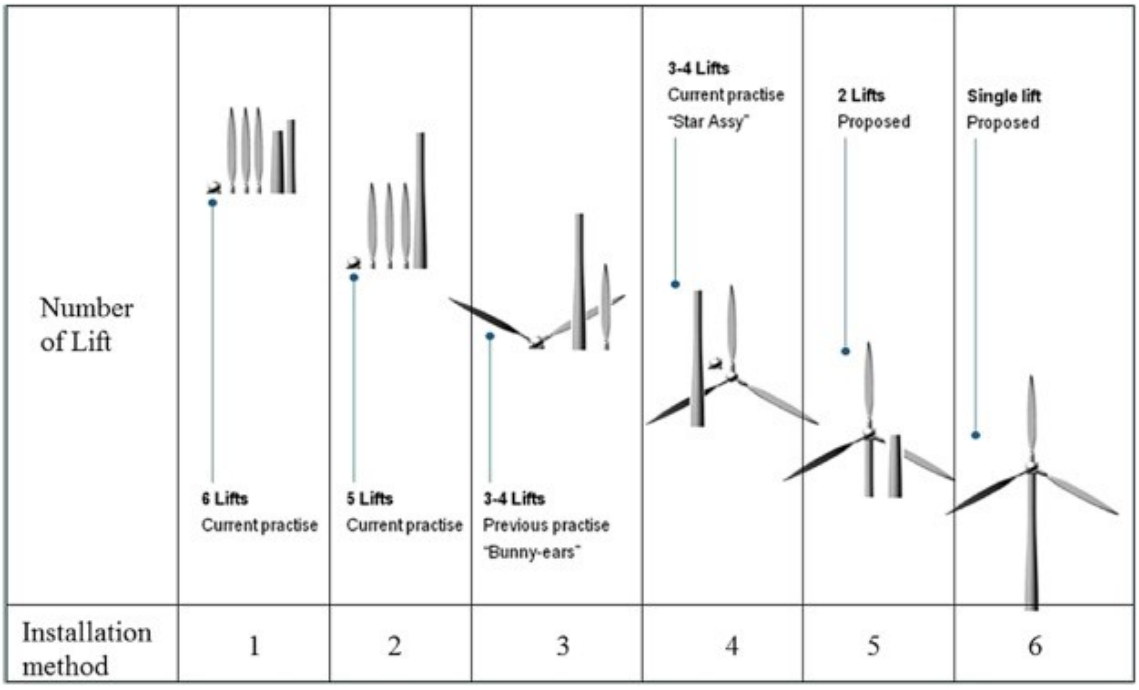

Figure 2.2: Different wind turbine installation methods [22].

2.2.1 Five or six lifts

For a five lift strategy, the tower is assembled in port and installed in one piece. A six lift strategy installs the two tower segments separately. The nacelle with hub is lifted on to the tower and the three blades are individually lifted and conncetd to the hub.

Individually stacking components reduce the required deck space on board and thus eases the transportation to the site. Using the five-lift strategy, a more efficient deck space usage is reached since the area occupied by the tower is only equal to the diameter once. More turbines can be transported in a single trip, reducing the installation costs. Moreover, separate installation can be performed with a crane that has less lift capacity compared to a massive single lift. Jiang et al.

(2021) noticed the trend that split installation with multiple components lifts is gaining popularity since the scale of wind turbines is increasing [23]. Verma et al. (2019) [24] also recognized that the split-type installation is preferred in industry. The pros and cons are listed as follows. Figure 2.3a illustrates the operation.

Industry	Method is popular due to increasing scale of turbines
Vessel requirements	Efficient deck space usage, blades can be stored in blade scaffolding
Lifting requirements	Lifting height is main driver, nacelle is heaviest component and deciding for lifting capacity
Electricity requirements	Power required to rotate the hub
Environmental	Large number of lifts required to complete operation, therefore operation is rather weather-sensitive

(a) Single blade installation [25].

(b) Lifting of Star Assy RNA assembly [26].

Figure 2.3: Multiple lift installation methods.

2.2.2 Three to four lifts with Star Assy

The hub and blades are pre-assembled to create a star. The nacelle without the hub is individually transported and the tower segments are either mated in port or separately transported and lifted. The advantages and disadvantages are summarized below. Figure 2.3b illustrates the installation operation.

Industry	Method has been applied, gaining popularity
Vessel requirements	Transportation is complex due to the shape of Star and inefficient deck space usage. Different trips might be necessary to collect new turbine parts
Lifting requirements	Lifting height is main driver. After grabbing the Star needs to be rotated 90 degrees to be installed
Electricity requirements	No power needed to rotate the hub
Loads	The aerodynamic loads are relatively large and hard to predict

2.2.3 Single and two lifts

For installation with a single lift the wind turbine needs to be fully pre-assembled. For a two lift strategy, the bottom tower segment, nacelle, hub and blades are all mated in port, while one tower segment is installed separately. The single or two lift installation method has not been applied widespread. Some demonstrator projects have been executed including two bottom-fixed projects; the Beatrice Demonstrator Project in 2007 and China's first offshore wind farm near the Shanghai Donghai Bridge in 2009.

The number of weather-restricted offshore lifts is reduced, which decreases the installation time and thus costs. The center of gravity of the single lift is relatively low. Lifting capacity, not lifting height, is the major challenge as the total mass of a fully assembled wind turbine is over 2500 t. The wind turbine can be installed with one large crane, but also with smaller two cranes from the side. Transportation of the turbine to the site is of concern. The complete turbine occupies a lot of deck space and the different turbines cannot be stacked together in a simple manner. Large installation cranes and vessels are thus needed. The benefits and advantages are summarized as follows.

Industry	Limited experience in industry, few demonstration projects have been executed
Vessel requirements	Transportation is challenging and limited to one or two turbines. Specially designed vessels are required for increasing scale of turbines raising costs
Lifting requirements	Lifting capacity is main driver
Time constraints	Limited number of offshore lifts, relatively quick on-site installation
Structural integrity	Connection between the tower and RNA is critical

(a) Single lift installation at Beatrice wind farm [20].

(b) Single lift installation at Hywind Scotland [27].

Figure 2.4: Single lift installation.

Several innovative installation concepts, such as the WindFloat Barge [28], the Ulstein fork-on and float-off procedure [29], the catamaran installation concept [30], and the large floating dock concept [31], were assessed and detailed in the literature review preceding this research [13]. While some of these concepts show potential, the majority is still in the early development phase. Therefore established methods are favored, also due to contractors' hesitance to adopt new installation techniques.

2.3 Single blade installation

In this section, an outline of the various stages associated with the single blade installation process is presented. Finally, the critical phase is discussed.

2.3.1 Mounting orientation

Single blade installation can be carried out in various blade orientations, including horizontal, vertical, and tilted. Both horizontal and vertical mounting necessitate electricity for hub rotation. In contrast, tilted orientation offers the advantage of a stationary rotor, eliminating the need for electricity during the installation process. However, a longer crane boom is required, as the blade is installed at a 60° angle, necessitating a reach that exceeds the hub's height. This could potentially impact the operation's feasibility, particularly considering the increasing size of wind turbines. Vertical mounting of the blade involves rotating the blade in the air before mating, as it is horizontally stacked on the deck. As a result, horizontal mounting is generally viewed as the most appropriate mounting orientation. The LT975 Blade Dragon lifting yoke is an example of a tool that can be used to install the blade at any angle on the hub [32]. The various mounting orientations can be seen in Figure 2.5.

(a) Horizontal orientation [33].

(b) Vertical orientation [32].

(c) Tilted orientation [23].

Figure 2.5: Three blade mounting orientations during single blade installation.

2.3.2 Installation procedure

The typical procedure for a horizontally-mounted single blade installation is described by Jiang et al. [33]. The marine operation is defined by the following sequence of steps:

1. **The positioning phase** in which the installation vessel is accurately positioned for the marine operation. Following this, the hub is rotated to facilitate blade mounting in a horizontal position.
2. **The lifting phase** in which the lifting tool, typically a blade yoke system, grasps the blade at its center of mass and elevates it to the hub's height.
3. **The alignment phase** involves aligning the blade root center with the hub center, with the assistance of a taglines system, if available. The crane slews the blade into the vicinity of the hub. If the relative blade root motion compared to the hub is within acceptable limits, the operation proceeds to the next phase. If alignment criteria are not met and the risk of hub collision increases, the operation is delayed for up to 30 minutes while the blade is held close to the hub. If weather conditions do not improve, the operation halts, and the blade is lowered back to the deck. The entire operation is then suspended until a suitable weather window arises.
4. **The mating phase** is critical and poses substantial impact risks. The main components include bolts, a longer guide pin, and flange holes. T-bolts are often utilized due to their low cost, ease of fabrication, and reproducibility. These bolts are evenly distributed. The guide pin serves as the primary connection point, entering the hub first through the flange hole. Subsequently, the bolts are mated with the other flanges. During this phase, the mating criteria, which are more stringent than the alignment criteria, are very important.

2.3.3 Critical phase

The critical phase of the operation is thus the mating phase between the blade root and the hub. The long and slender blades are susceptible to wind loads, especially at large hub heights. The consequences of an accidental impact in the final mating phase were studied [24]. A three-dimensional finite element model for the blade root and T-bolts was created and the impact

assessment showed severe bending and plastic deformation of the guide pin bolt in case of an impact force. The blade root has to withstand the maximum flapwise and edgewise moments and torques exerted by the aerodynamic forces. Therefore root is usually the thickest part of the blade. Damage to the blade root is thus of concern. Once the structural integrity of the blade is compromised due to impact, the blade will be lowered to deck for inspection. In worst case the blade needs to be completely replaced or repaired on deck. Even if after inspection another attempt to install the blade can be performed, the marine operation will delayed which would wastes valuable weather window and induces higher costs.

Verma et al. (2019) defined two possible impact scenarios. The first being collision due to relative motion along the longitudinal axis of the blade [24]. The guide pin and bolts will be affected. The bolts are generally designed to withstand axial loads during operations. The second scenario is impact the due to motions along the transverse axis of the lifted blade. This sideways motion damages the guide pin bolts and, since the bolts are not designed for transverse loads, will be the most critical. Moreover the blade root laminate could be affected, which can not always be visually observed.

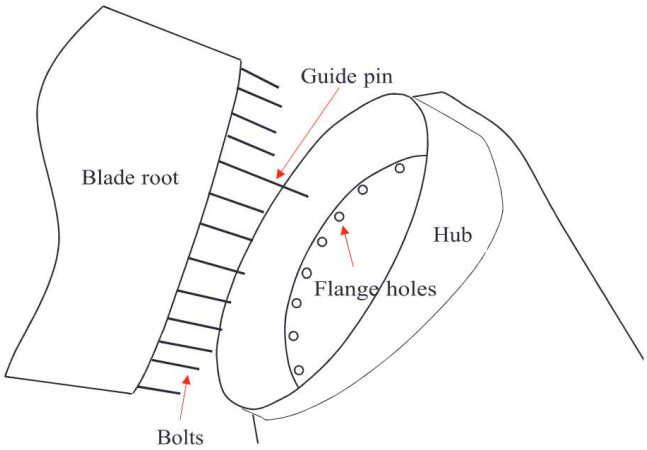

Figure 2.6: Schematic of main components during final mating phase [33].

To summarize, installation operations are highly sensitive to environmental conditions, weather-restricted and time-limited. Marine operations are categorised based on the type of crane support and the structure on which the load is lifted. Floating-to-floating installations have been conducted in the past, but only as single-lift operations in sheltered areas using a large semi-submersible vessel. On-site floating-to-floating installations have not yet been performed.

Various installation methods have been employed in the industry for installing the rotor nacelle assembly. Single blade installation is advantageous because it optimizes deck space and speeds up transportation. Furthermore, the stick-built method is the most commonly used installation method, making it appealing for contractors who are reluctant to adopt new installation techniques. The mating phase is considered the most critical due to the significant operating height and the small motion criteria. This procedure involves aligning the blade's guiding pin with the corresponding hole in the hub and securing the connection using flanges and bolts. The guiding pin ensures accurate alignment between the blade and hub, while the flanges provide a strong mechanical connection between the two components. Finally, the bolts are tightened to maintain a secure connection and prevent any movement between the blade and hub. The floating-to-floating installation poses several challenges, including the susceptibility of the crane vessel to wave loads, the motion of the wind turbine due to waves, and the relative motion between the two entities that poses an additional threat to single blade installation.

Chapter 3

Method and software

This chapter presents the methodology. An overview and flowchart of the steps taken, along with some background information on equations of motion, response spectra, and spectral parameters, are presented in Section 3.1. Additionally, Section 3.2 offers an overview of the software utilized in the analysis.

3.1 Methodology

To compare the workability of a floating-to-floating operation with that of a fixed-to-fixed operation, the operation is modeled in the frequency domain. Previous research by Slootweg ([34]) has indicated that the frequency domain provides comparable results to the time domain for a floating-to-fixed lift. To compare the workability of a floating-to-floating operation with that of a fixed-to-fixed operation, the operation is modeled in the frequency domain. As this study serves as a preliminary investigation on the single blade installation of floating wind turbines using a floating vessel, the frequency domain is deemed adequate, although it has some limitations. The limitations and assumptions are discusses in Section 4.4. Background on potential wave theory can be found in Appendix 10.

Initially, the hydrodynamic coefficients, added mass, radiation damping, and wave forces of the semi-submersible floating wind turbine and the crane vessel are computed using linearized potential flow equations, as outlined in Section 3.1.1. A single-body computation is conducted for both bodies, followed by a multibody model in which the two bodies are in proximity to simulate the floating-to-floating operation. The resulting global motion is compared to analyze the effect of the presence of the vessel on the wave-induced motion of the floating wind turbine and vice versa.

Motions RAOs are combined with wave spectra and wave contours to arrive at significant and maximum motions. The response spectrum is thus determined, as described in Section 3.1.2. The relative motion is computed for different environmental conditions and tested to the relative motion criteria, as described in Chapter 5. Finally, the workability of the operation is evaluated for a specific site and compared to that of a fixed-to-fixed operation.

The methodology is summarized in Figure 3.1. Overall, this modeling approach provides valuable insights into the hydrodynamics of multibody floating structures, which is crucial for successful offshore floating-to-floating operations and enables quantification of a floating-to-floating lift.

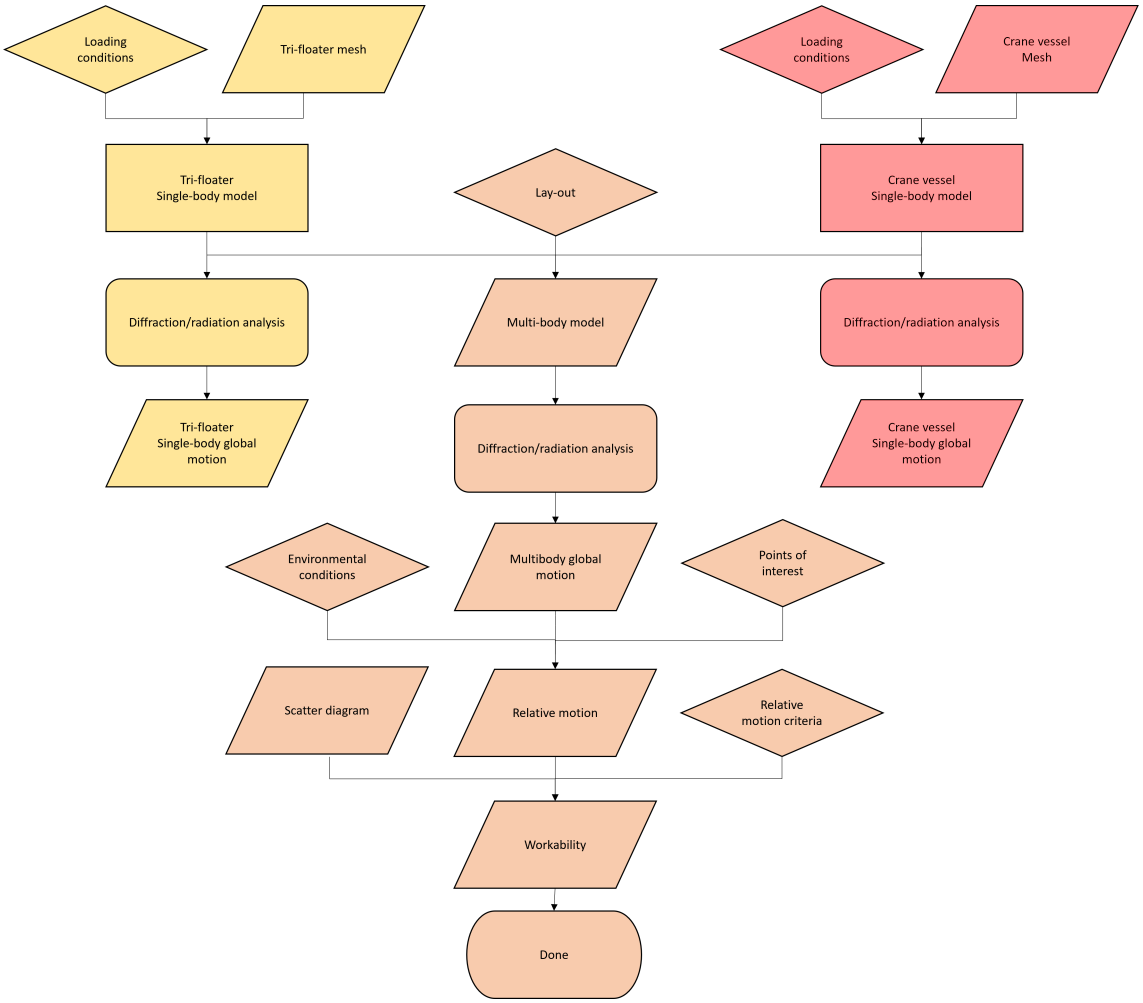

Figure 3.1: Methodology flowchart.

3.1.1 Equations of Motion

To analyze the behavior of a floating wind turbine and a vessel, it is necessary to formulate the Equations of Motion (EoMs), which are a set of coupled differential equations and which describe the response of a body as a result of excitation forces. The EoMs for the structure from the wave-body interaction originate from Newton's second law.

$$\sum_{k=1}^{6} M_{jk}\ddot{x}_k(t) = F_j(t) \quad j = 1, \ldots, 6 \tag{3.1}$$

In which M is the mass of the body, F the external force on the body and $\ddot{x}$ the acceleration. The subscripts j and k can be thought of as a mass associated with a force on the body in the j direction due to a unit acceleration in the k direction. The external force is determined by wave loads. The linear wave-body problem in regular waves consists of two subproblems:

- **Diffraction problem** is formulated when a rigid body is exposed to incoming waves with a certain frequency. This results in a scattered wave field around the object.
- **Radiation problem** is related to the presence of a rigid body in forced motions. The body oscillates with a frequency in calm water generating waves that radiate away from the body.

From the former the wave excitation loads are obtained. These consist of the Froude–Krylov force, which is a force introduced by the unsteady pressure field generated by undisturbed waves and the diffraction force, originating from the the floating body disturbing the waves. From the latter

problem the added mass, damping and restoring terms are obtained, also known as the the hydrostatic loads. Together they result in linear wave-induced motions, accelerations and structural loads. The Equations of Motion for a rigid body in the frequency domain are displayed as:

$$-\boldsymbol{\omega^2}(\boldsymbol{M}+\boldsymbol{A}(\boldsymbol{\omega}))\boldsymbol{X}(\boldsymbol{\omega})+\boldsymbol{i\omega B}(\boldsymbol{\omega})\boldsymbol{X}(\boldsymbol{\omega})+\boldsymbol{CX}(\boldsymbol{\omega})=\boldsymbol{F^{ext}}(\boldsymbol{\omega}) \tag{3.2}$$

in which $\mathbf{M}$ is the mass matrix, $\mathbf{A}$ the added mass matrix, $\mathbf{B}$ the structural damping matrix and $\mathbf{K}$ the structural stiffness matrix. The system motion is represented in vector $\mathbf{X}(\omega)$ and the excitation forces acting on the system are displayed in $\mathbf{F}^{\text{ext}}(\omega)$.

3.1.2 Response to waves

In order to simulate the dynamics of a floating wind turbine and a crane vessel in an offshore wind farm, it is necessary to obtain a comprehensive understanding of the ocean waves in the surrounding environment. Wind-generated deep water waves are characterized as having short crests, being irregular, and unpredictable. To model irregular wave elevations, a statistical description using linear wave theory is used. An irregular wave elevation is described by the superposition of constant sinusoidal regular waves:

$$\zeta(t,x)=\sum_{j=1}^{N}A_j\sin\left(\omega_j t-k_j x+\epsilon_j\right) \tag{3.3}$$

In which $\zeta(t,x)$ is the irregular wave elevation dependent on both time and place, A_j the wave amplitude, ω_j the wave frequency, k_j the wave number and ϵ_j the random phase angle between 0 and 2 π. The wave amplitude can be expressed in terms of an amplitude spectrum S_ζ, describing the distribution of wave energy across different frequencies.

$$\frac{1}{2}A_j^2=S_\zeta\left(\omega_j\right)\Delta\omega \tag{3.4}$$

In which $\delta\omega$ is a constant frequency step in the spectrum. The Response Amplitude Operator (RAO) is a frequency dependent transfer function which predicts the linear response of a floating body to the wave elevation. The RAO relates the body motion amplitude η_a to the wave elevation amplitude ζ_a:

$$RAO(\omega)=\frac{\eta_a(\omega)}{\zeta_a(\omega)} \tag{3.5}$$

The wave response spectrum $S_{\eta\eta}$ describes the maximum response of a body to waves across different frequencies. It is derived from the wave amplitude spectrum $S_{\zeta\zeta}$ and the response amplitude operator (RAO):

$$\begin{aligned}S_{\eta\eta}(\omega)\mathrm{d}\omega&=\frac{1}{2}\eta_a^2(\omega)\\&=\left|\frac{\eta_a(\omega)}{\zeta_a(\omega)}\right|^2\cdot\frac{1}{2}\zeta_a^2(\omega)\\&=\left|\frac{\eta_a(\omega)}{\zeta_a(\omega)}\right|^2\cdot S_{\zeta\zeta}(\omega)\mathrm{d}\omega\end{aligned} \tag{3.6}$$

$$S_{\eta\eta}(\omega)=|RAO|^2\cdot S_{\zeta\zeta}(\omega) \tag{3.7}$$

This research considers twelve degrees of freedom, including the surge, sway, and heave motions, as well as the roll, pitch, and yaw rotations for the semi-submersible floating wind turbine and the crane vessel. These degrees of freedom are further specified in Chapter 4.

3.1.3 Spectral parameters

The workability is based on the maximum allowable motions of the vessels, which can be estimated from the wave response spectrum and the transfer functions between the waves and the vessels. The Most Probable Maximum (MPM) is a statistical measure of the maximum of a variable with the highest probability of occurring within a certain reference period. For this study, the MPMs are determined for a 3-hour reference period. This is a common value in the offshore industry as it is the approximate time in which a sea state is assumed to be constant. The calculation of the MPM amplitude is based on the Rayleigh distribution model and the non-exceedance interval. The non-exceedance interval is the probability that a given value will not be exceeded within the reference period.

$$MPM = \sigma \cdot \sqrt{1 - 0.368^{\frac{1}{N}}} \tag{3.8}$$

$$N = \frac{3 \cdot 3600}{T_z} \tag{3.9}$$

In which σ is the variance and T_z is the zero-crossing period of the motion response spectrum.

3.2 Software

A panel mesh model of both the vessel and the Tri-floater are first created in Rhino 7. The orientation of the bodies in the multibody model is decided in AUTOCAD. The hydrodynamic coefficients, added mass, radiation damping and wave forces in the frequency domain are computed using WAMIT. WAMIT is a radiation/diffraction software developed by MIT used to analyze wave interactions with offshore structures in the frequency domain. First, the radiation and diffraction velocity potential on the body surface for the specified modes, frequencies and wave headings are determined, followed by the hydrodynamic loads and coefficients. Afterwards, the velocities and pressures on the body surface and the hydrodynamic coefficients, motions and forces are computed. Post-processing of the hydrodynamic databases resulting from the single-body models and the multibody model is conducted in Python. The different softwares and their versions used are indicated in Table 3.1.

Description	**Software**	**Version**
Mesh	Rhino	7
Orientation	AUTOCAD	8
Radiation / diffraction analysis	WAMIT	3.9
Post-processing	Python	7

Table 3.1: Software used throughout this research

Chapter 4

Model and assumptions

This chapter provides a summary of the frequency domain multi-body model and enumerates the primary assumptions of the model. Section 4.1 details the equipment and units employed in this research. Section 4.2 outlines the orientation and distance between the equipment in the multibody model. Section 4.3 introduces the global and local coordinate systems and degrees of freedom of the model, while Section 4.4 outlines the model's assumptions. Finally, Section 4.5 presents the site location, the site specifications, as well as the wave environment.

4.1 Unit description

In this research a 15MW wind turbine blade is installed on a semi-submsersible floating wind turbine with a large monohull crane vessel. In this section, the blade is described, the semi-submersible floating wind turbine and vessel specifications are given and the points of interest are outlined.

4.1.1 Blade

The IEA 15 MW reference wind turbine blade is selected for this research. A market overview for different large scale wind turbines prior to this selection is presented in the literature review [13]. The wind turbine characteristics are presented in Table 4.1. The blade is 117 m long and has a mass of 65 t.

Wind turbine model	Year	Hub Height (m)	Blade Length (m)	Mass (t)	RNA Mass (t)	Nacelle Mass (t)	Tower Mass (t)
NREL 15 MW	2020	150	117	65	1446	1251	1211

Table 4.1: IEA 15 MW wind turbine characteristics [35].

4.1.2 Floating offshore wind turbine

The GustoMSC Tri-floater is a floating offshore wind turbine consisting of a modular three-column semi-submersible with a single turbine positioned at the center of one of the sides. The concept is known for its shallow draft, modular structure, and gentle motions, as the natural periods of the structure do not fall within the range of wave periods. Originally introduced in 2003 [36], the concept underwent iterations and improvements over time. Initially, the turbine was located at the center of the floater to avoid the need for additional ballast to counterbalance its weight. However, in later designs, the turbine was relocated to enhance accessibility for installation and maintenance. In 2021 Det Norske Veritas (DNV) succesfully completed the concept verification and released a statement of feasibility, confirming technical feasibility [37]. Currently, GustoMSC employs two installation strategies for the Tri-floater, which involve either onshore installation using a crane from the quayside or installation in a sheltered area of the port using a jack-up vessel [38]. Subsequently, the structure is water ballasted on site, increasing its draft from 8.5 m in the harbor to an operational draft of 20 m [38].

Table 4.2 summarizes the dimensions and general properties of the floater for the design with a reference NREL 15 MW turbine [35]. Figure 4.1a provides an impression of the design concept, while the Rhino mesh used throughout this research, provided by GustoMSC, is shown in Figure 4.1b.

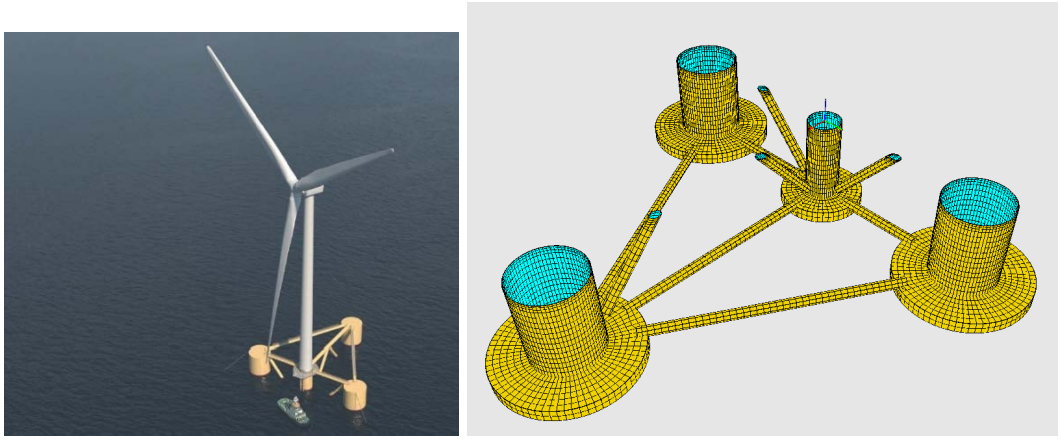

(a) Tri-floater [38]. (b) Tri-floater mesh.

Figure 4.1: GustoMSC Tri-floater.

Property	**Unit**	**Value**
Length overall	m	94
Beam overall	m	104
Operational draft	m	20
Harbor draft	m	8.5
Floater weight approx.	t	5000
Hub height above SWL	m	143
Wind turbine weight approx.	t	2300
Design survival H_s	m	13.5
Design operational H_s	m	10

Table 4.2: Tri-Floater design characteristics for configuration with the NREL 15 MW turbine [38].

4.1.3 Crane vessel

The GustoMSC Ensis heavy lift crane vessel is specifically designed for the offshore wind installation market. The monohull crane vessel is optimized for monopile and jacket installation but can also be used for other offshore construction activities due to its multi-purpose design. In order to reduce the effects of wave-induced motion on the crane vessel, a relatively large monohull crane vessel is selected for this study. If the feasibility of the floating-to-floating blade installation with the Ensis is proven, a smaller and more cost-effective monohull crane vessel can be explored.

The dimensions and general properties are summarized in Table 4.3. Figure 4.2a provides an impression of the design concept, while the Rhino mesh used throughout this research, provided by GustoMSC, is shown in Figure 4.2b.

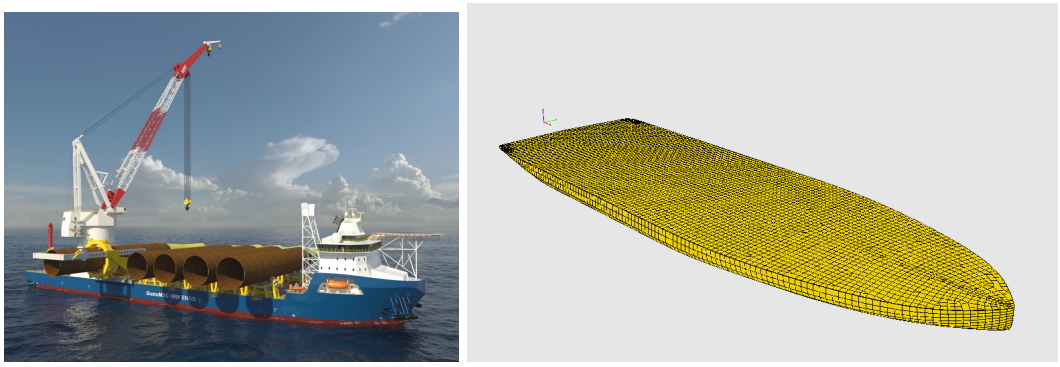

(a) Crane vessel [39]. (b) Crane vessel mesh.

Figure 4.2: GustoMSC Ensis.

Property	Unit	Value
Length	m	200
Width	m	55
Depth	m	17
Draft	m	8-11
Deadweight	t	> 30 000

Table 4.3: Ensis design characteristics [39].

4.1.4 Loading conditions

The motion is analysed for a single loading condition. The Vertical Center of Gravity (VCG), the Transverse Center of Gravity (TCG) and the Longitudinal Center of Gravity (LCG) the transverse metacentric height (GM_T), the longitudinal metacentric height (GM_L), the radius of gyration in roll (k_{xx}), pitch (k_{yy}) and yaw (k_{zz}) are selected. The Tri-floater is assumed to be freely floating, and under operational draft of 20 m.

To establish conservative yet realistic results, the least favorable loading condition for the crane vessel is selected from prior research [34]. The loading condition is a combination of a low draft and a high metacentric height.

Property	Unit	Value
Displacement	t	15000
Draft	m	20

Table 4.4: Tri-Floater loading conditions.

Property	Unit	Value
Displacement	t	40000
Draft	m	5.6

Table 4.5: Crane vessel loading conditions.

4.2 Unit lay-out

In this section the orientation of the Tri-floater with respect to the crane vessel and the horizontal distance between the two units is described.

4.2.1 Unit orientation

The relative motion of the crane tip and the hub are influenced by the relative position of the crane vessel with respect to the Tri-floater. Two installation orientations are considered; a stern-to-hub-orientation, displayed in Figure 4.3a and a side-to-hub orientation, shown in Figure 4.3b.

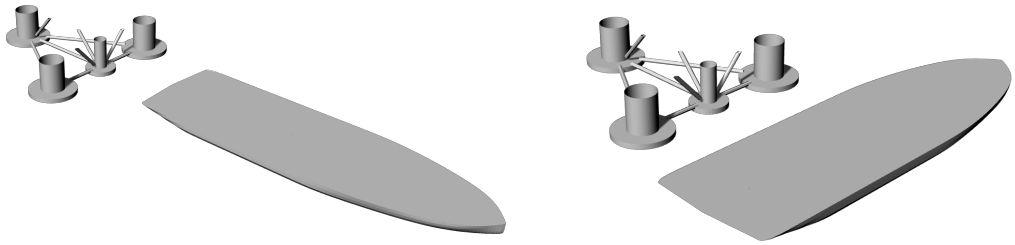

(a) Stern-to-hub orientation. (b) Side-to-hub orientation.

Figure 4.3: Different orientations for the Tri-floater and crane vessel.

Both orientations have advantages and disadvantages. Lifting heavy objects over the stern side of a vessel is generally considered safer as it provides more stability along the longitudinal axis of the ship compared to lifting it over the side which is along the transverse axis and therefore subject to more movement and instability. From an operational perspective, it is more common to lift heavy objects over the side of the vessel. This is because the side of the vessel is usually more accessible and provides a larger working area compared to the stern side. Additionally, the crane is located on the side, making it easier to lift and transfer heavy objects. The side-to-hub orientation can help to reduce the wave loads on the Tri-floater during the installation process, since the vessel can shield the floater. The slewing speed of the crane is 15 minutes at a rate of 90°. This is particularly important in time-restricted operations, as reducing the overturning moment can improve the efficiency and thus costs of the installation process. The time spent on slewing is dependent on the positioning of the blades on deck. Deck space is thus factor to take into consideration.

In both orientations, the distance from the mooring lines to the vessel is taken into account. The Tri-floater utilizes either catenary or semi-taut mooring, with the mooring lines attached at an angle of 45° to the top of the columns. Based on the vessel's dimensions, draft, and the requirements of the mooring system, a minimum horizontal distance between the Tri-Floater and the crane vessel of approximately 30 m is needed to maintain a safe clearance from the vessel to the mooring lines. A safety margin of an additional 10 meters is also included in this number to ensure a sufficient level of safety.

4.2.2 Distance between units

The horizontal distance between the Tri-floater and the crane vessel depends on the crane type, crane hoist and subsequent crane outreach. The crane is a pedestal crane. The crane has three different hoists; the main hoist, the auxiliary hoist, and the whip hoist. As the blade is not directly connected to the crane hook, rigging and equipment height of 25 m is taken into account. For single blade installation of the NREL 15MW blade with a blade mass of 65 t and a length of 117 m, lifting height rather than crane capacity is the biggest issue. The main hoist is not able to lift the wind turbine to the required height. However, for a side-to-hub orientation, both the auxiliary and whip hoists suffice.

The crane load curve is the connection between the crane load and the crane outreach, for every crane hoist. For a stern-to-hub orientation, only the whip hoist has sufficient crane outreach to install the turbine, while both the auxiliary and whip hoist suffice for a stern-to-side orientation.

The auxiliary hoist is selected due to its larger loading capacity. Although the required loading capacity for a wind turbine blade is low, the stick-build installation process and multi-purpose design philosophy of the crane vessel indicate that other wind turbine components, including heavier ones like the hub, could also be installed in a similar operation. This can save time, thus costs, during the installation process, as the auxiliary hoist can be used to install multiple elements of the wind turbine without having to switch to a different hoist. This is especially useful if the weather window of the operation is small.

All in all, a side-to-hub orientation with use of the auxiliary hoist is selected for this research. This

indicates that the crane vessel undergoes a 270° rotation to align the crane on the portside of the crane vessel with the hub. The horizontal distance between the Tri-floater and the crane vessel is 61 m.

4.3 Coordinate system

The global motions are defined in terms of the Degrees of Freedom (DoFs). The DoFs are a set of independent displacements and rotations that eventually give a complete overview of the displaced position and orientation of a body [40]. The six global motions are presented in Table 4.6.

Description	Name	Symbol
Translation along X-axis	Surge	x
Translation along Y-axis	Sway	y
Translation along Z-axis	Heave	z
Rotation around X-axis	Roll	ϕ
Rotation around Y-axis	Pitch	θ
Rotation around Z-axis	Yaw	ψ

Table 4.6: Global motion components.

4.3.1 Global coordinate system

The following global coordinate system is applicable:

- The X-axis is defined as positive from the centre of the wind turbine
- The Y-axis is defined as positive from the centre of the wind turbine to the portside
- The Z-axis is defined as positive upwards from the waterline

A counterclockwise rotation is defined as positive.

4.3.2 Local coordinate systems

Next to the global coordinate system, two local coordinate systems are defined.

Tri-floater coordinate system

Next to the global coordinate system, two local coordinate systems are defined. The origin of the body-fixed Tri-floater coordinate system is similar to the origin of the global coordinate system. The x_f-, y_f- and z_f- axis align with the X-, Y- and Z-axis.

Crane vessel coordinate system

The body-fixed crane vessel coordinate system is defined:

- The x_v-axis is defined as positive from the stern to the bow of the vessel
- The y_v-axis is defined as positive from the centre line of the vessel to the port side
- The z_v-axis is defined as positive upwards from the waterline

4.3.3 Definition of degrees of freedom

All DoFs in the multi-body model are listed table 4.7 and visualised in 4.4. The motions of the floater and vessel are given at the Centre of Gravity (CoG) of each body.

The wave heading is defined as positive rotating about the global Z-axis. The global and local coordinate systems, as well as the global wave headings are visualized in 4.4. The global coordinate system is indicated in grey, the body-fixed Tri-floater coordinate system in blue and the body-fixed crane vessel coordinate system is indicated in red.

Element	Modeled as	DoF	Degrees of Freedom
Vessel	Rigid body	6	$x_v, y_v, z_v, \phi_v, \theta_v, \psi_v$
Floater	Rigid body	6	$x_f, y_f, z_f, \phi_f, \theta_f, \psi_f$

Table 4.7: Degrees of freedom for the multibody model.

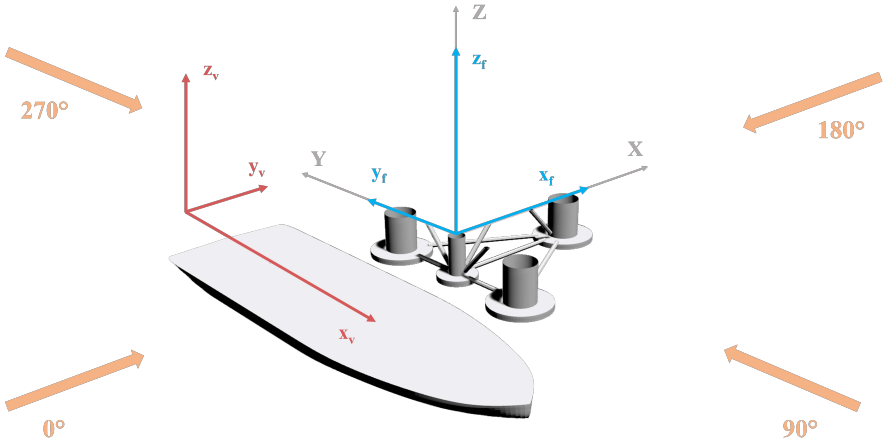

Figure 4.4: Axis orientation of the multi-body model, with global wave directions indicated.

4.3.4 Points of interest

The initial location of the points of interest, with respect to the Still Water Level (SWL) of the Tri-floater and crane vessel respectively, are documented in Table 4.8.

Point	Unit	$\mathbf{x_v}$	$\mathbf{y_v}$	$\mathbf{x_v}$
Crane tip	m	52.5	88.5	168
		$\mathbf{x_v}$	$\mathbf{y_f}$	$\mathbf{x_f}$
Hub	m	0	0	143

Table 4.8: Points of interest.

The x-, y- and z-coordinates of the Tri-floater hub are denoted as x_H, y_H and z_H. The x-, y- and z-coordinates of the crane tip are denoted as x_{CT}, y_{CT} and z_{CT}. A schematic impression of the translations of the crane tip and hub are displayed in Figure 4.5.

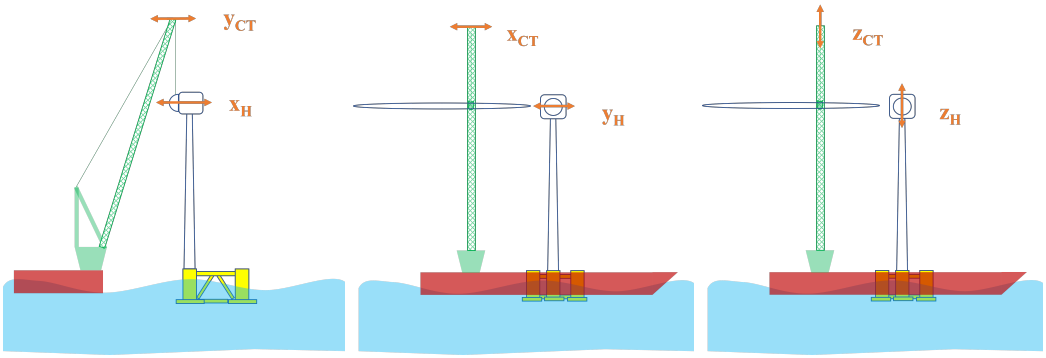

(a) Hub and crane tip translations in global surge.

(b) Hub and crane tip translations in global sway.

(c) Hub and crane tip translations in global heave.

Figure 4.5: Schematic overview of the relative translations.

4.4 Assumptions

The most important assumptions of the model are listed:

- The Tri-floater and crane vessel are assumed to be rigid bodies.
- The wind turbine tower and crane are assumed to be rigid, meaning no deformation takes place and as a result, the distance from the point of interest to the CoG of the crane vessel and Tri-floater remains constant.
- The weight of the blade, blade gripper and other auxiliary measures is small compared to the weight of the crane vessel and therefore the motion behavior of the crane vessel is not influenced by the presence of these elements.
- The selected motion compensation systems are fully operational within the provided compensation range.
- The blade is rigidly connected to the crane vessel, meaning that the taglines are assumed to be always under tension. If the blade is rigidly connected, the taglines controlling the blade's position are always under tension, causing the blade to move with the crane as one unit. This allows for the analysis of the relative motion between the hub and the crane tip.
- The Tri-floater is assumed to be freely floating, with the weight of the mooring system considered but not the stiffness damping matrix.
- The hydrodynamic damping of the vessel is assumed to be 5% of the critical damping in the roll direction.
- The hydrodynamic damping of the floater is assumed to be 5% of the critical damping in the heave, roll and pitch direction.
- The model does not account for non-linear damping, such as quadratic drag coefficients or Morrison damping.
- A linear wave excitation frequency range is considered.
- Only first order wave forces are taken into account.
- The crane vessel is assumed to be equipped with a Dynamic Positioning (DP) system compensating for wave drift forces.
- Wind and current loads on the Tri-floater and crane vessel are neglected.
- The fluid is irrotational, inviscid and incompressible.
- The waves are assumed to be small.
- The wave steepness is assumed to be small.
- The waves are assumed to be regular.

4.5 Environmental conditions

In this section the environmental input conditions, the site specifications and wave environment are described.

4.5.1 Environmental input

According to DNV [15] important ocean-related environmental phenomena which may influence the operational limitations and restrictions are waves and swell, currents and tide. This research only takes first-order wind-generated waves into account. The environmental input conditions are shown in Table 4.9.

Property	Unit	Range	Step size
Wave direction	°	0 - 345	15
Wave frequency	rad/s	0 - 2	0.01
Significant wave height	m	1 - 8	1
Peak period	s	1 - 11	1

Table 4.9: Environmental conditions.

4.5.2 Site

A generic site with moderate conditions from the EU-funded Lifes50+ project is selected for this study [41]. Site B is located in the Gulf of Maine area in the United States of America (USA). The site is located in the North Atlantic ocean, 65 km east from Portland. Moderate site conditions apply with respect to the magnitude of the 50-year extreme wave height extreme wind speed. The site parameters are shown in Table 4.10. A parameter with a 50-year return periods indicates that the probability of occurrence within one year is $\frac{1}{50} = 0.02 = 2\%$. This site is considered a reasonable starting point for investigation of floating-to-floating lifts. The coordinates of the central point of the rectangle indicated in Table 4.11 and the site is displayed in Figure 4.6.

Property	Unit	Value
Distance from shore	km	9
Water depth	m	150
50-yr significant wave height	m	10.9
50-yr significant peak period range	s	9 - 16

Table 4.10: Site parameters [41].

Site	Latitude	Longitude
Gulf of Maine	43°33'22.4"N	69°27'08.7"W

Table 4.11: Site coordinates [41].

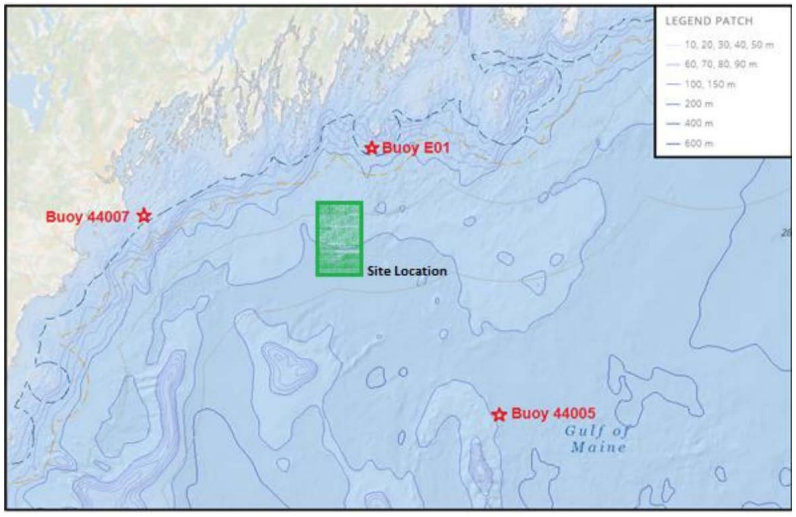

Figure 4.6: Site location [41].

The scatter diagram in Figure 4.7 is used as input data for the model, providing the significant wave height (H_s) and peak period (T_p) values that are used to simulate the environmental conditions. The scatter diagram represents the probability of a H_s - T_p pair occurring at the site, based on historical buoy data collected between 2003 and 2015. For certain H_s - T_p pairs the probability has no value, indicating that the waves with these characteristics do not appear at the site.

		Peak period (s)								
		1 < Tp < 2	2 < Tp < 3	3 < Tp < 4	4 < Tp < 5	5 < Tp < 6	6 < Tp < 7	7 < Tp < 9	9 < Tp < 10	Tp > 11
Significant wave height (m)	Hs < 1	0.03%	4.69%	7.29%	7.02%	3.91%	5.91%	13.49%	6.27%	0.08%
	1 < Hs < 2		0.00%	0.92%	6.64%	6.85%	7.32%	7.90%	8.36%	0.16%
	2 < Hs < 3			0.00%	0.09%	0.55%	2.71%	2.91%	3.32%	0.15%
	3 < Hs < 4				0.00%	0.01%	0.12%	1.11%	1.04%	0.08%
	4 < Hs < 5						0.00%	0.19%	0.47%	0.04%
	5 < Hs < 6							0.02%	0.21%	0.01%
	6 < Hs < 7								0.08%	0.01%
	7 < Hs < 8								0.02%	0.01%
	Hs > 8								0.00%	0.00%

Figure 4.7: Scatter diagram [41].

		Distribution (%)
Wave directionality (°)	0	1.01%
	30	1.10%
	60	1.83%
	90	16.01%
	120	38.00%
	150	29.51%
	180	8.30%
	210	1.73%
	240	0.94%
	270	0.44%
	300	0.51%
	330	0.83%

(a) Wave distribution.

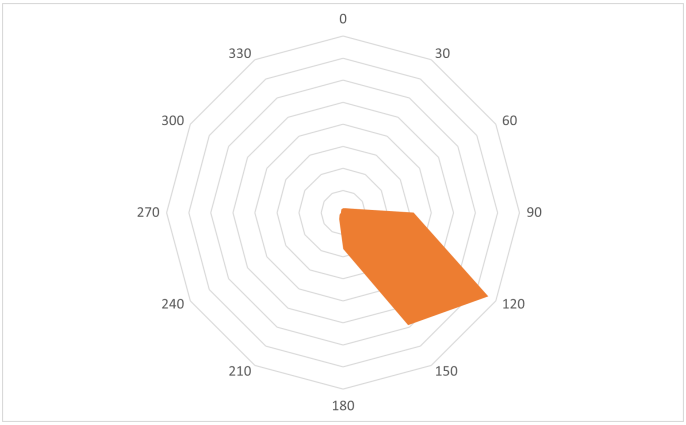

(b) Wave rose.

Figure 4.8: Wave directionality [41].

4.5.3 Wave environment

Ocean waves can be described by the wave spectrum under the assumption that the sea is a stationary random process. For analyses of marine operation the spectrum is assumed time-invariant for a period of 3 hours [42]. This is also known as the short-term description of the sea.

In 1973 the Joint North Sea Wave Observation Project (JONSWAP) was created to describe storms of limited fetch, which indicates that the wave energy is limited by the size of the wave generation area [43]. In practice sea states are seldom fully developed due to non-linear wave interactions. The JONSWAP spectrum is a widely used spectral model for describing ocean waves in a statistical sense, and is based on measurements of wave data collected in the North Sea. However, it has been found to be applicable to many other ocean regions, including the North Atlantic. These parameters include the significant wave height H_s, peak wave period T_p, and spectral shape parameters that describe the shape of the wave energy spectrum which can be adjusted to match the local wave conditions. The JONSWAP spectrum is described in Appendix 10.

By using the JONSWAP spectrum to describe the wave conditions at the specific location in the North Atlantic, it is possible to estimate the statistical distribution of wave heights and periods, as well as other wave characteristics to decide whether the floating-to-floating operation can be executed.

Chapter 5

Relative motion criteria

The workability of the installation operation is determined using relative motion criteria, which are explained in this chapter. Section 5.1 outlines the criteria used during the mating phase, and Section 5.2 explores the motion compensation systems that can expand upon these criteria, ultimately drawing a conclusion regarding the relative motion criteria in this research.

5.1 Mating criteria

Firstly, the maximum allowable motion during the critical mating phase is determined. Research conducted by de Leeuw in partnership with Van Oord BV [44] has established that the maximum distance between the hub center and blade root center should not exceed 0.2 m. If the relative motion between the two, referred to as d_{hb}, is less than this threshold, the mating procedure can be performed safely without causing any damage to the guide pins and bolts.

This mating criteria referred to pertain specifically along the blade's transverse axis, as illustrated in Figure 5.1. The distance between the hub and blade root center is denoted as d_{hb}. The motion of the blade in the crane vessel local coordinate system in sway is denoted as y_{bl}, while the motion of the blade in heave is represented as z_{bl}.

Unlike the research conducted by De Leeuw [44], which assumes a fixed hub, this study takes the motion of the hub into account. The relative motion criteria governing the transverse axis are affected by the hub surge, blade sway, hub heave, and blade heave, as defined in Section Chapter 4.3.

It is assumed that the relative motion criteria along the blade's longitudinal axis is comparable to that of the transverse axis. This assumption implies that the relative motion between the blade's surge in the crane vessel local coordinate system and the hub's sway in the Tri-floater local coordinate system must not exceed 0.2 m.

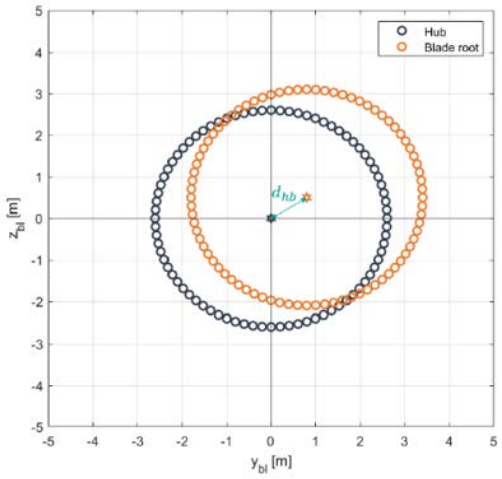

Figure 5.1: Position of the blade root center with respect to the center of the hub[44].

5.2 Relative motion criteria

Subsequently, the relative motion criteria for the floating-to-floating operation is derived. The criteria for mating described earlier can be expanded by incorporating motion compensation systems. It is assumed that the blade position is controlled with three compensation systems during the lifting procedure: a horizontal tagline to the wind turbine, two horizontal taglines to the crane boom, and a heave compensator. Each compensation system works in one direction of the blade motions, x-, y-, or z-direction. The strokes of these compensation systems are ultimately responsible for the relative motion criteria between the hub and the crane tip.

Research conducted by Slootweg [34] in collaboration with GustoMSC examined the compensation stroke of horizontal taglines. Their findings revealed that the stroke depends on the amount of pre-displacement of the taglines that the crane geometry permits. If the blade has been pre-displaced by 2 m, the mating criteria will be met, resulting in a compensation stroke of ± 1 m.

Heave compensators are extensively researched and commonly used in the offshore industry. These compensators are mounted between the hook and the load, allowing them to compensate for any heave motion. They are capable of compensating for a range of 0.5 to 5 m [45], which results in a maximum compensation stroke of ± 2.5 m.

Figure 5.2, Figure , and Figure 5.4 demonstrate the operational principles of the horizontal taglines and the heave motion compensator.

Figure 5.2 demonstrates the compensation provided by the horizontal taglines attached to the crane boom and heave compensator, which is necessary due to Tri-floater pitch and crane vessel roll.

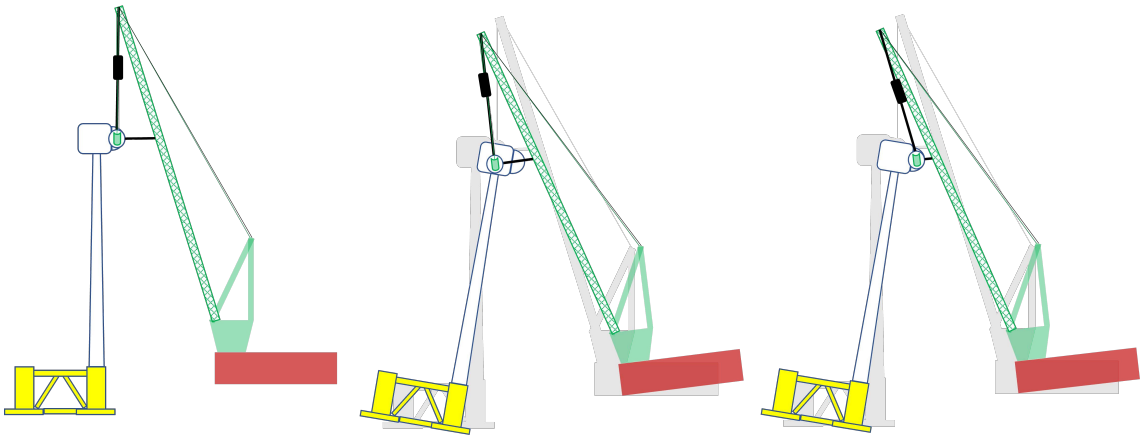

Figure 5.2: Back view of the operation, compensation as a consequence of vessel roll and Tri-floater pitch.

Figure 5.3 depicts the compensation provided by the horizontal tagline attached to the wind turbine and heave compensator, which are required due to Tri-floater roll and crane vessel pitch.

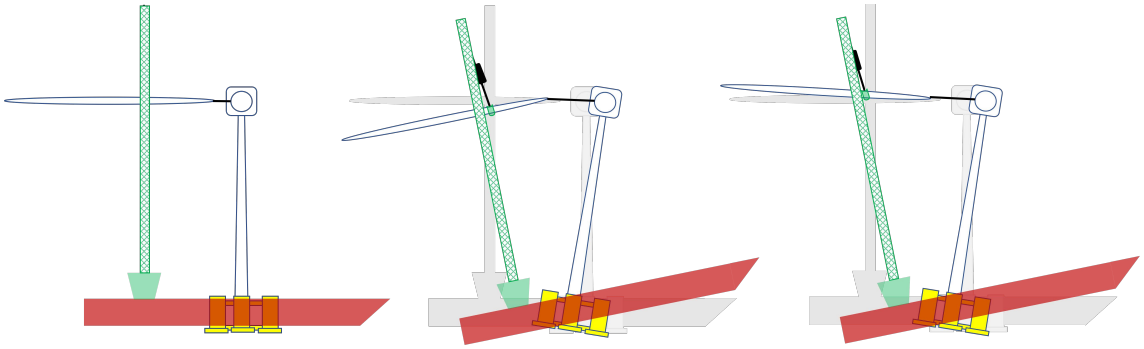

Figure 5.3: Starboard side view of the operation, compensation as a consequence of vessel pitch and Tri-floater roll.

Figure 5.4 offers a top-down perspective of all horizontal taglines in operation, necessitated by Tri-floater and crane vessel yaw.

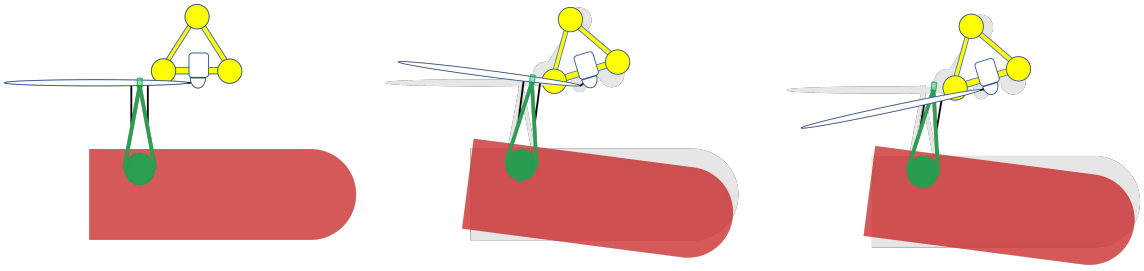

Figure 5.4: Top view of the operation, compensation as a consequence of vessel and Tri-floater yaw.

In summary, this research focuses on the relative motion between the crane tip and hub as an indicator of the relative motion between the blade root and the hub. The relative motion criteria is three-fold, depending on the relative motion between the crane tip and the hub:

- Global x-direction: x_H - $y_{CT} < \pm$ 1 m, dependent of the stroke of the horziontal tagline towards the wind turbine

- Global y-direction: y_H - $x_{CT} < \pm$ 1 m, dependent of the stroke of the two horizontal taglines to the crane boom
- Global z-direction: z_H - $z_{CT} < \pm$ 2.5 m, dependent of the stroke of the heave compensator

Adhering to these relative motion criteria is expected to ensure a safe and successful floating-to-floating operation.

Chapter 6

Results: motions and workability

This chapter provides the results from the model. Initially, Section 6.1 presents the natural frequencies of both the Tri-floater and the vessel, followed by a discussion of the wave forces, moments, and global motion RAOs in Section 6.2. This section provides an elaboration on the differences between the multibody and single-body models. Section 6.3 presents the relative motion between the crane tip and the hub. Section 6.4 displays the spectral analysis of the motion response and the workability for a floating-to-floating lift at the selected site.

6.1 Natural frequencies

The Tri-floater and crane vessel possess a restoring force in the form of hydrostatic stiffness in heave, roll, and pitch. As a result, only natural frequencies in these degrees of freedom are present. It is important to take these natural frequencies into account because resonance can occur when a body is stimulated with the same frequency as its eigenfrequency. Table 6.1 displays the uncoupled natural frequencies and natural periods of both the Tri-floater and the crane vessel.

	heave	roll	pitch
Tri-floater			
Natural frequency (rad/s)	0.4	0.2	0.2
Natural period (s)	17	31	31
Vessel			
Natural frequency (rad/s)	0.7	0.6	0.7
Natural period (s)	9	11	10

Table 6.1: Natural frequencies and natural periods for the Tri-floater and the crane vessel.

6.2 Absolute motion

This section presents the results of the single-body and multi-body analysis for the Tri-floater and crane vessel. It includes the wave forces and global motion RAOs, which are provided and compared between the single-body and multi-body models.

6.2.1 Tri-floater

Wave forces

Figure 6.1 compares the wave force in heave and the wave moments in roll and pitch between the multi-body and single-body models of the Tri-floater for a 0, 90 and 180° wave direction. As defined in Chapter 4, the wave orientation is defined in the global coordinate system, whereas the Tri-floater motions are expressed in the Tri-floater local coordinate system.

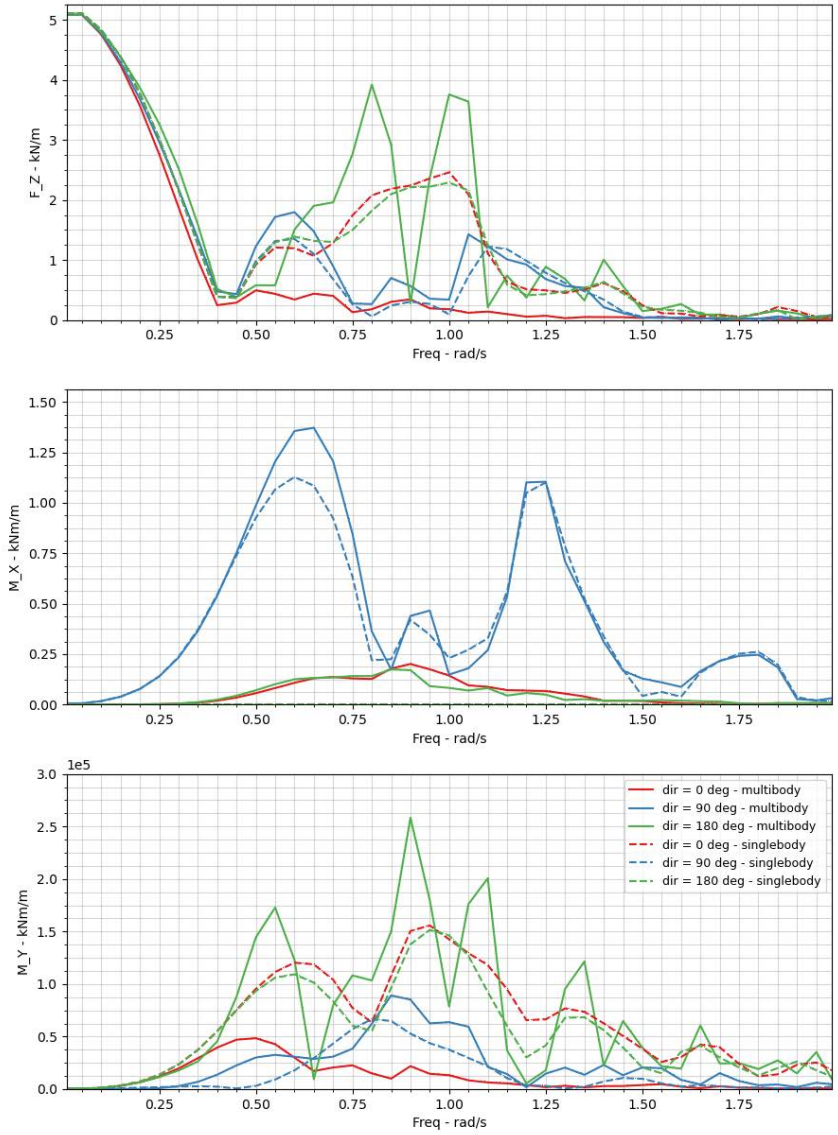

Figure 6.1: Comparison of wave forces acting on the Tri-floater in the single-body and multi-body models for heave, roll and pitch for waves at an incidence angle of 0, 90, and 180°.

Initially, the single- and multi-body models are validated by investigating the anticipated behavior of the Tri-floater relative to the wave direction. It is expected that the moment around the y-axis M_y will be greater than the motion around the x-axis M_x for a wave direction of 0° and 180°, while the opposite is expected for a 90° wave direction. This is because the wave moment around the y-axis is mainly influenced by the wave force in x-direction, while the wave moment around the x-axis is affected by the wave force in the y-direction. Figure 6.1 shows that the trends observed are in line with these expectations.

Upon examining the wave forces, it can be concluded that the two Tri-floater and crane vessel are in sufficiently close proximity to experience significant hydrodynamic interactions. Differences between the single-body and multibody model are observed.

In the multibody model with a 0° wave direction, the crane vessel is situated between the incoming waves and the Tri-floater. Therefore the crane vessel shields the Tri-floater from the waves, reducing its exposure to the waves. This shielding effect only occurs for wave frequencies larger than 0.25 rad/s. One way to conceptualize this is by considering the inverse relationship between wave length and wave frequency. When wave frequencies are lower and wave lengths are longer, the incoming

wave lifts both the vessel and the Tri-floater completely without any interaction between the two bodies. For higher wave frequencies and thus shorter wave lengths, the crane vessel reduces the wave loads on the floater by attenuating the incoming waves. Due to this effect, the wave moment around the y-axis M_y in the multibody model is significantly lower than the wave moment in the single-body model for this wave orientation. This effect is also observed in the wave force in the z-direction, represented by F_z.

In the multibody model with a 180° wave direction, the Tri-floater is first exposed to the full force of the wave. Afterwards, the waves encounter the crane vessel. The waves are radiated, diffracted, and reflected by the crane vessel. The Tri-floater experiences a reflected wave from the vessel which may result in an additional displacement of the Tri-floater in the opposite direction of the initial incoming wave. Due to this effect, the wave moment around the y-axis M_y exhibits considerably higher peaks in the multibody model compared to the single-body model for this wave orientation.

In the multibody model with a wave direction of 90°, there is no shielding or reflection as the Tri-floater and crane vessel are approached simultaneously by the wave. Nevertheless, the crane vessel still radiates waves and diffracts the incoming wave, leading to increased wave forces on the Tri-floater. The observed increase in the wave moment around the x-axis M_x could be attributed to these two effects. The absence of wave reflection leads to a relatively small increase in wave moment.

In the multibody model, the shielding effect for 0° waves, the reflection effect for 180° waves, and the radiation and diffraction effect for 90° waves can be observed. One should note that the radiation effect is probable to be present for every wave direction in the multibody model.

Global motion RAO

Subsequently, the global motion RAOs of the Tri-floater at the center of gravity in heave, roll and pitch are computed.

The four effects observed in the wave forces RAOs, shielding, reflection, radiation and diffraction, are also observed in the global motion RAOs. In the multibody model with a 180° wave direction, the pitch motion displays significantly higher peaks. The shielding effect is observed for a 0° wave direction in heave, while change in amplitude is observed for waves with a 90° wave direction in roll.

The resonance peak in pitch at the Tri-floater natural frequency of 0.2 rad/s, has a considerably large amplitude for all wave directions in the multibody model compared to the single-body model. For this frequency, the wave force in the z-direction and wave moment around the y-axis do not exhibit any differences compared to the single-body model. Therefore, the trend is expected to be similar to that observed in the single-body model. It is worth noting that the resonance peak is also present in the multibody surge RAO, given the existence of surge-pitch coupling in the Tri-floater. A possible explanation for this result may be the lack of adequate implementation of viscous damping. The model only incorporates viscous damping as a percentage of critical damping, since non-linear viscous effects are not taken into account in the linear model. These results therefore need to be interpreted with caution for lower wave frequencies. Since this inaccuracy has not been observed for wave frequencies within the typical wave spectrum, it is not expected that this observation will significantly influence the relative motion response.

6.2.2 Crane vessel

Wave forces

Figure 6.2 compares the wave force in heave and the wave moments in roll and pitch between the multi-body and single-body models of the crane vessel for a 0, 90 and 180° wave direction. As defined in Chapter 4, the wave orientation is defined in the global coordinate system, whereas the crane vessel motions are expressed in the crane vessel local coordinate system. It is important to note that a 90° environmental direction corresponds to head waves on the crane vessel, while 0 and 180° represent beam waves on the crane vessel, as the body-fixed vessel origin is rotated with respect to the global origin.

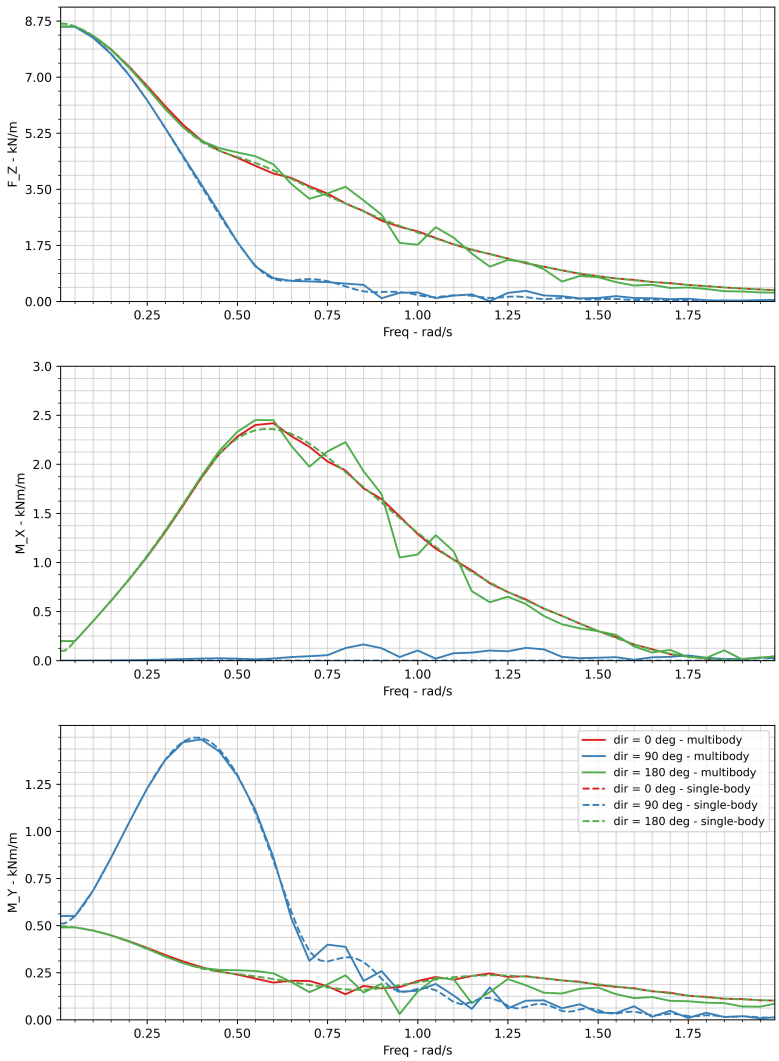

Figure 6.2: Comparison of wave forces acting on the crane vessel in the single-body and multi-body models for heave, roll and pitch for waves at an incidence angle of 0, 90, and 180°.

Again, the single- and multi-body models are validated by investigating the anticipated behavior relative to the wave direction. The wave moment around the y-axis M_y is significantly greater for a 90° wave direction than for 0 and 180° waves, while the opposite is true of the the wave moment around the x-axis M_x. Due to the vessel's symmetry along the longitudinal axis, the wave force in the z-direction F_z is much smaller for head waves than the wave force resulting from beam waves.

In the multibody model with a 180° wave direction, the Tri-floater is situated between the incoming waves and the crane vessel. Contrary to the shielding effect observed in Section 6.2.1, the wave forces are not attenuated by the presence of the Tri-floater. The crane vessel is observed to have a more significant influence on the wave-induced motion of a semi-submersible floating offshore wind turbine than vice versa. A possible explanation for this might be that the braced structure of the Tri-Floater, with the buoyancy columns and heave plates makes it permeable to waves. Conversely, the solid vessel is more resistant to incoming waves, resulting in a larger impact on the Tri-Floater's wave-induced motion. Furthermore, the crane vessel's length is larger than the Tri-floater's breadth. A possible explanation for the peaks observed for this wave direction in F_z and M_x is that the cylindrical structure causes wave to diffract in multiple directions, Compared to the diffraction observed from the crane vessel (which can be considered as a flat wall)

In the multibody model with a 0° wave direction, the crane vessel is encountered first by the waves, and then the Tri-floater. The wave force RAOs do not show significant differences for the

multibody model compared to the single-body model. It seems possible that the reflection and radiation effect are insignificant.

It is possible that this diffraction effect also causes the peaks in the multibody model for a 90° wave direction in M_y.

Global motion RAO

Subsequently, the global motion RAOs of the crane vessel at the center of gravity in heave, roll and pitch are computed. The motion RAOs for surge, sway and yaw are also computed.

The presence of the Tri-Floater has relatively little impact on the motion of the crane vessel in heave, roll and pitch. The roll motion RAO exhibits roughly similar behavior for beam waves from both 0° and 180° environmental directions. It is probable that wave diffraction influences the crane vessel motion for a 180° wave environment, as more peaky trends are observed in heave and pitch.

The resonance peak in roll at the eigenfrequency of 0.5 rad/s falls within the wave frequency range of a typical wave spectrum, which is probable to cause significant motion in sway. This resonance is larger for a 0° wave direction than for a 180° wave direction.

In summary, the most notable difference in motion behaviour between the multibody and single-body model of the Tri-floater is caused by the shielding and reflection effect due to the presence of the vessel. Overall, single-body and multibody models show good agreement in this simulation for the crane vessel, and the presence of the Tri-Floater has relatively little effect on its motion. These findings suggests that the multibody model is correctly implemented and can be used as a reliable tool for further linear investigations.

6.3 Relative motion

The importance in a floating-to-floating lift is the relative motion between the crane tip and the hub, rather than the absolute motion of the two bodies. The relative motion RAOs in surge, sway and heave are shown in Figure 6.3. The relative motion depends on the absolute motion and the phase of the hub and the crane tip. The absolute motion RAOs of all degrees of freedom of the hub and crane tip and the relative phase for a wave direction of 0 ° are also computed.

The relative phase indicates how much the motion of the hub leads or lags behind the motion of the crane tip. If the relative phase is zero, it means that the motion of the hub and crane tip are perfectly synchronized. If the relative phase is positive, it means that the motion of the hub leads the motion of the crane tip, and if the relative phase is negative, it means that the motion of the hub lags behind the motion of the crane tip. This happens when wave at the crane tip arrives before it arrives at the hub due to their respective positions.

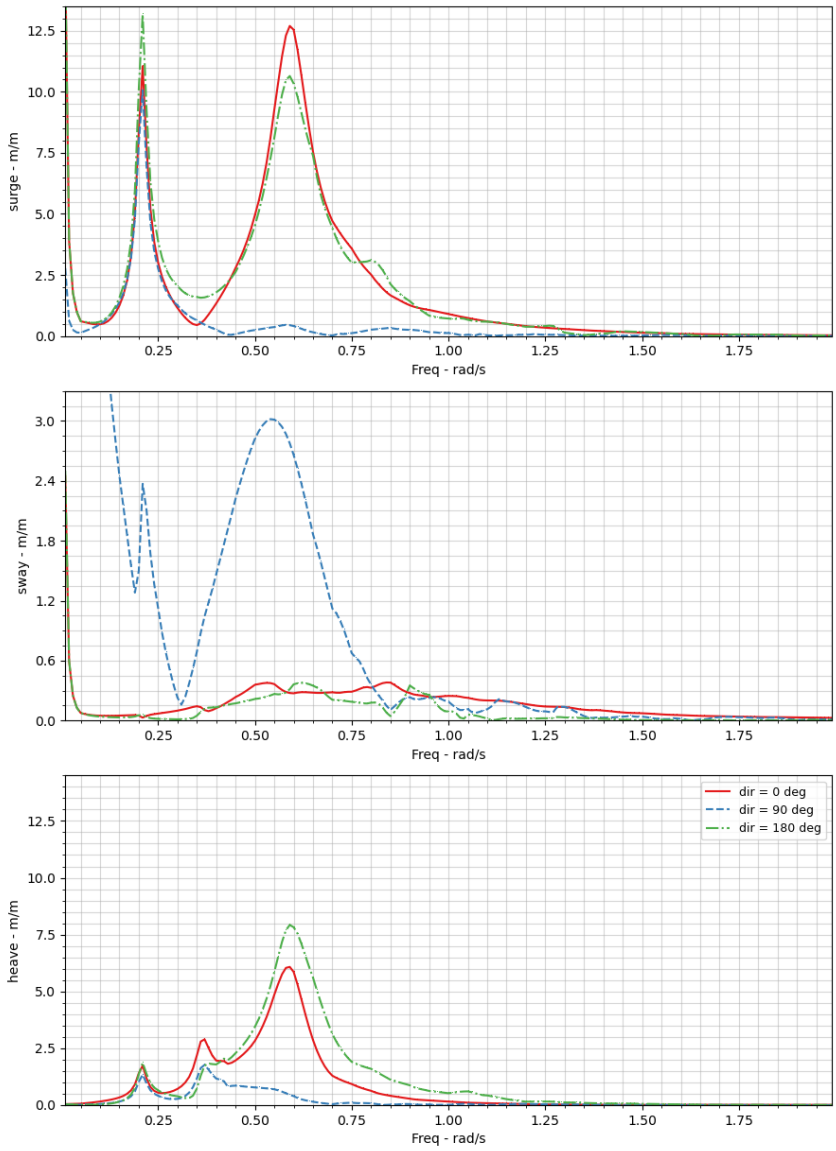

Figure 6.3: Relative translation RAOs between crane tip and hub.

The relative motion in surge is influenced by the Tri-floater surge, pitch and yaw, and crane vessel sway, roll and yaw. The relative surge peak of 12.5 m at a wave frequency of 0.6 rad/s originates from the crane tip roll angle of 4.5° at the natural frequency of the crane vessel. Since the crane tip is located far from the CoG of the vessel, where the motion RAOs are initially computed, even a slight rotation of the crane vessel can lead to a significant displacement at the crane tip. As explained in Section 6.2.1, the large resonance peak in surge originating from the Tri-floater pitch at a wave frequency of 0.2 rad/s does not affect the relative motion response between the crane tip and hub since the frequency is outside of the wave frequency range. The relative surge is larger for a 0° wave direction that 180° wave direction, originating from the larger roll angle for the crane vessel for this wave direction.

The relative motion in sway is influenced by the Tri-floater sway, roll and yaw, and crane vessel surge, pitch and yaw. The roll angle of Tri-floater causes sway for a wave frequency of 0.2 rad/s, but again outside the wave frequency range so it will not influence the response spectrum.

The relative motion in heave is influenced by the the pitch and roll of both the Tri-floater and crane vessel. The reflection and shielding effect of the Tri-floater different wave directions can be observed at wave frequencies between 0.5 and 1.25 rad/s. The heave resonance peak originates

from the crane vessel roll, in which it can be seen that heave for a 180° wave direction is larger than for 0° waves. If the wave comes from the windward side of the crane vessel, a 180° direction, more heave is expected on that side of the vessel compared to the leeward side. This is because the windward side experiences a higher wave amplitude, which means that the peak of the wave is higher relative to the vessel's position. The leeward side, on the other hand, experiences a lower wave amplitude, which means that the trough of the wave is shallower relative to the vessel's position. This creates a phase difference between the two sides, resulting in more motion on the windward side.

6.4 Motion response and workability

This section presents the results of relative motion response between Tri-floater and crane vessel in surge, sway and heave under a conservative assumption. Subsequently, the worst performing motion is selected to provide the workability of the floating-to-floating operation. Lastly, the workability for the floating-to-floating operation is compared to that of a fixed-to-fixed, and floating-to-floating operation.

6.4.1 MPM in relative surge, sway and heave

The relative motion response spectrum is dependent on the relative motion RAO and the JONSWAP wave spectrum. The MPMs for the relative surge, sway and heave are displayed in Figure 6.4, Figure 6.5, and Figure 6.6 respectively. The values are conservative in two ways. The MPM values are computed for the upper limit of the H_s - T_p range provided by the scatter diagram described in Chapter 4. The values displayed on the H_s - T_p diagram correspond to the highest MPM values obtained from all wave directions. The motion of the Tri-floater and crane vessel is affected by the direction of incoming waves, with the crane vessel being particularly sensitive to wave direction due to the RAO value at its natural frequency being larger in roll than in pitch and within the linear wave excitation range. Depending on the direction of the waves, it is possible to observe smaller relative motions than what is shown. A more thorough analysis that considers the wave direction and the wave rose at the site is analysed and evaluated in Chapter 7.

		Peak period (s)								
		1 < Tp < 2	2 < Tp < 3	3 < Tp < 4	4 < Tp < 5	5 < Tp < 6	6 < Tp < 7	7 < Tp < 9	9 < Tp < 10	10 < Tp < 11
Significant wave height (m)	Hs < 1	0.00	0.03	0.13	0.38	0.90	1.86	4.79	5.68	6.05
	1 < Hs < 2		0.05	0.26	0.72	1.68	3.72	9.58	11.37	12.10
	2 < Hs < 3			0.39	1.08	2.41	5.20	14.37	17.05	18.14
	3 < Hs < 4				1.44	3.21	6.75	19.37	22.74	24.19
	4 < Hs < 5						8.44	24.41	31.32	30.78
	5 < Hs < 6							29.39	40.19	40.51
	6 < Hs < 7								49.20	50.59
	7 < Hs < 8								57.71	60.89

Figure 6.4: Relative amplitude in surge, for all H_s - T_p pairs in the scatter diagram of site.

		Peak period (s)								
		1 < Tp < 2	2 < Tp < 3	3 < Tp < 4	4 < Tp < 5	5 < Tp < 6	6 < Tp < 7	7 < Tp < 9	9 < Tp < 10	10 < Tp < 11
Significant wave height (m)	Hs < 1	0.00	0.02	0.08	0.20	0.52	0.95	1.65	1.82	1.88
	1 < Hs < 2		0.05	0.16	0.37	0.97	1.91	3.29	3.63	3.77
	2 < Hs < 3			0.24	0.56	1.34	2.86	4.94	5.45	5.65
	3 < Hs < 4				0.74	1.78	3.81	7.00	7.26	7.54
	4 < Hs < 5						4.76	9.27	9.68	9.48
	5 < Hs < 6							11.57	12.17	11.82
	6 < Hs < 7								14.70	14.44
	7 < Hs < 8								17.13	17.10

Figure 6.5: Relative amplitude in sway, for all H_s - T_p pairs in the scatter diagram of site.

		Peak period (s)								
		1 < Tp < 2	2 < Tp < 3	3 < Tp < 4	4 < Tp < 5	5 < Tp < 6	6 < Tp < 7	7 < Tp < 9	9 < Tp < 10	10 < Tp < 11
Significant wave height (m)	Hs < 1	0.00	0.01	0.06	0.23	0.55	1.22	3.14	3.73	3.97
	1 < Hs < 2		0.02	0.12	0.41	1.06	2.42	6.29	7.45	7.94
	2 < Hs < 3			0.17	0.61	1.57	3.36	9.43	11.18	11.90
	3 < Hs < 4				0.81	2.09	4.28	12.79	14.90	15.87
	4 < Hs < 5						5.36	16.21	20.62	20.17
	5 < Hs < 6							19.60	26.55	26.37
	6 < Hs < 7								32.59	32.78
	7 < Hs < 8								38.28	39.31

Figure 6.6: Relative amplitude in heave, for all H_s - T_p pairs in the scatter diagram of site.

Figure 6.4, Figure 6.5, and Figure 6.6 indicate if the MPM values exceed the relative motion criteria as defined in Chapter 5.1. A few differences can be observed. For wave conditions where the significant wave height is between 1 and 2 and the peak period is between 5 and 6, the relative surge does not satisfies the relative motion criteria, while the relative sway and heave do meet the criteria. All in all, it can be concluded floating-to-floating operation is constrained by the surge motion, as the relative motion is largest under the conservative assumption.

6.4.2 Workability

The workability of the floating-to-floating operation is therefore dependent on the relative surge amplitude. The ability to perform a floating-to-floating operation depends on the surge amplitude, as shown by Figure 6.7, which displays the probability of occurrence for each combination of significant wave height and peak period and whether the criteria for workability are met. The workability for the floating-to-floating operation is 31%.

		Peak period (s)									
		1 < Tp < 2	2 < Tp < 3	3 < Tp < 4	4 < Tp < 5	5 < Tp < 6	6 < Tp < 7	7 < Tp < 9	9 < Tp < 10	10 < Tp < 11	
Significant wave height (m)	Hs < 1	0.03%	4.69%	7.29%	7.02%	3.91%	5.91%	13.49%	6.27%	0.08%	22.94%
	1 < Hs < 2		0.00%	0.92%	6.64%	6.85%	7.32%	7.90%	8.36%	0.16%	7.56%
	2 < Hs < 3			0.00%	0.09%	0.55%	2.71%	2.91%	3.32%	0.15%	
	3 < Hs < 4				0.00%	0.01%	0.12%	1.11%	1.04%	0.08%	
	4 < Hs < 5						0.00%	0.19%	0.47%	0.04%	
	5 < Hs < 6							0.02%	0.21%	0.01%	
	6 < Hs < 7								0.08%	0.01%	
	7 < Hs < 8								0.02%	0.01%	
		0.03%	4.69%	8.21%	13.66%	3.91%					30.50%

Figure 6.7: Probability distribution for a floating-to-floating operation with a conservative approach.

6.4.3 Comparison to other operations

Workability for the fixed-to-fixed operation

A fixed-to-fixed operation exhibits a workability of 87%, when applying the generally accepted environmental limit of a significant wave height of 2 m is utilized for the fixed-to-fixed operation., as illustrated in Figure 6.8.

		Peak period (s)									
		1 < Tp < 2	2 < Tp < 3	3 < Tp < 4	4 < Tp < 5	5 < Tp < 6	6 < Tp < 7	7 < Tp < 9	9 < Tp < 10	10 < Tp < 11	
Significant wave height (m)	Hs < 1	0.03%	4.69%	7.29%	7.02%	3.91%	5.91%	13.49%	6.27%	0.08%	48.69%
	1 < Hs < 2		0.00%	0.92%	6.64%	6.85%	7.32%	7.90%	8.36%	0.16%	38.15%
	2 < Hs < 3			0.00%	0.09%	0.55%	2.71%	2.91%	3.32%	0.15%	
	3 < Hs < 4				0.00%	0.01%	0.12%	1.11%	1.04%	0.08%	
	4 < Hs < 5						0.00%	0.19%	0.47%	0.04%	
	5 < Hs < 6							0.02%	0.21%	0.01%	
	6 < Hs < 7								0.08%	0.01%	
	7 < Hs < 8								0.02%	0.01%	
		0.03%	4.69%	8.21%	13.66%	10.76%	13.23%	21.39%	14.63%	0.24%	86.84%

Figure 6.8: Probability distribution for a fixed-to-fixed operation.

Workability for the floating-to-fixed operation

The motion between the crane tip of the crane vessel and a stationary hub determines the workability of the floating-to-fixed operation. Figure 6.9 displays the motion in surge. When comparing the results to the results from the floating-to-floating operation in surge from Figure 6.4, two observations are made. The relative motion between the crane tip and stationary hub is smaller than the relative motion between the crane tip and moving hub. This slight differences in relative motion does not influence the workability of the operation. The workability for the floating-to-fixed operation is 31% , similar to that of the floating-to-floating operation.

		Peak period (s)								
		1 < Tp < 2	2 < Tp < 3	3 < Tp < 4	4 < Tp < 5	5 < Tp < 6	6 < Tp < 7	7 < Tp < 9	9 < Tp < 10	10 < Tp < 11
Significant wave height (m)	Hs < 1	0.00	0.02	0.13	0.38	0.85	1.79	4.52	5.35	5.69
	1 < Hs < 2		0.05	0.25	0.71	1.64	3.56	9.04	10.71	11.38
	2 < Hs < 3			0.38	1.07	2.38	5.02	13.56	16.06	17.07
	3 < Hs < 4				1.43	3.17	6.46	18.32	21.41	22.76
	4 < Hs < 5						8.08	23.15	29.52	28.95
	5 < Hs < 6							27.93	37.91	38.01
	6 < Hs < 7								46.44	47.40
	7 < Hs < 8								54.49	56.97

Figure 6.9: Relative motion for a floating-to-fixed operation.

To summarize, this chapter provides a detailed analysis of the workability of different lifting operations for a floating wind turbine. The study shows that the relative surge is a limiting factor for the floating-to-floating operation. Furthermore, the workability of the floating-to-floating operation is only 31%, which is much lower than that of a fixed-to-fixed lift, with a workability of 87%. The floating-to-fixed operation has a similar workability to that of the floating-to-floating operation. These findings are based on the conservative assumption that the MPM values for the worst-performing wave directions are guarding the workability.

Chapter 7

Sensitivity study: wave direction

This chapter offers a sensitivity study concerning wave direction and draws a parallel to fixed-to-fixed and floating-to-fixed operations. Section 7.1 analyzes the dependence of relative motion on wave directionality. Section 7.2 does the same for floating-to-fixed operations.

Instead of the conservative approach as used in the previous chapter, the dependency of relative motions on wave direction is discussed.

7.1 Floating-to-floating operation

Firstly, the dependency of the relative motion on the wave direction for the floating-to-floating operation is analysed. Figure 7.1 highlights the wave orientation with respect to the Tri-floater and the crane vessel. The relative surge, sway and heave are all defined in the global coordinate system.

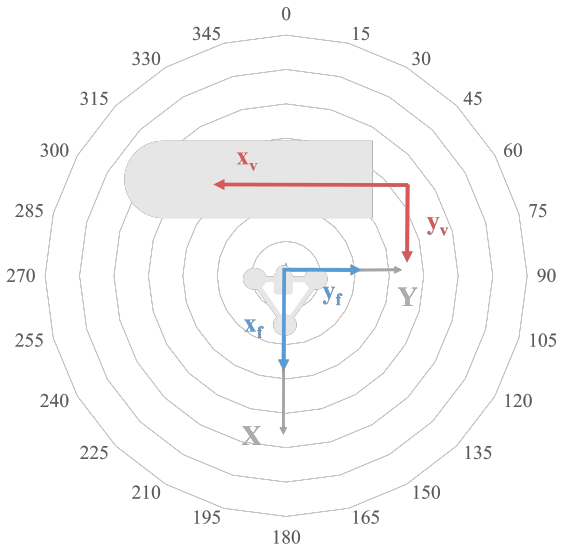

Figure 7.1: The model with respect to the global wave direction.

The wave direction dependency for relative surge, sway and heave is depicted in Figure 7.2d. respectively. These figures serve the purpose of examining the wave direction that yields the greatest amount of relative motion. Each wave rose displays the relative motion in surge, sway or heave for a significant wave height of 1 m and peak period ranging from 1 to 11 seconds. The magnitude of relative motion increases with higher peak periods, as depicted by the lighter colors on the visualization. The radial axis depicts the absolute magnitude of the relative motion. The wave

rose graphs are divided into sectors, with each sector representing a different global wave direction. By overlaying all of the wave roses into a single graph, Figure 7.2d allows for the identification of the limiting wave direction of the entire operation for this particular significant wave height.

Firstly, Figure 7.2a shows the wave direction dependency for relative surge, translation along the grey global X-axis in Figure 7.1. It is apparent from this figure than a 0° environmental direction results in the largest relative surge. The relative surge is observed within a constrained range of wave directions, spanning from 330 to 30° and from 150 to 210°. Secondly, Figure 7.2b shows the wave direction dependency for relative sway, translation along the grey global Y-axis in Figure 7.1. From the figure, it can be seen that the relative motion for sway is large when the relative motion in surge is small, and vice versa. Thirdly, Figure 7.2c shows the wave direction dependency for relative heave, translation along the out-of-plane global Z-axis. It is noteworthy that the heave wave direction dependency is governed by the relative surge wave rose. However, it is also observed that, contrasting to relative surge, the relative heave is larger for waves with a 180° environmental orientation than for waves with a 0° wave orientation. This is again in line with the findings presented in Section 6.3, as the relative heave for 180° waves is greater than for 0° waves due to the phase differences between the windward and leeward side.

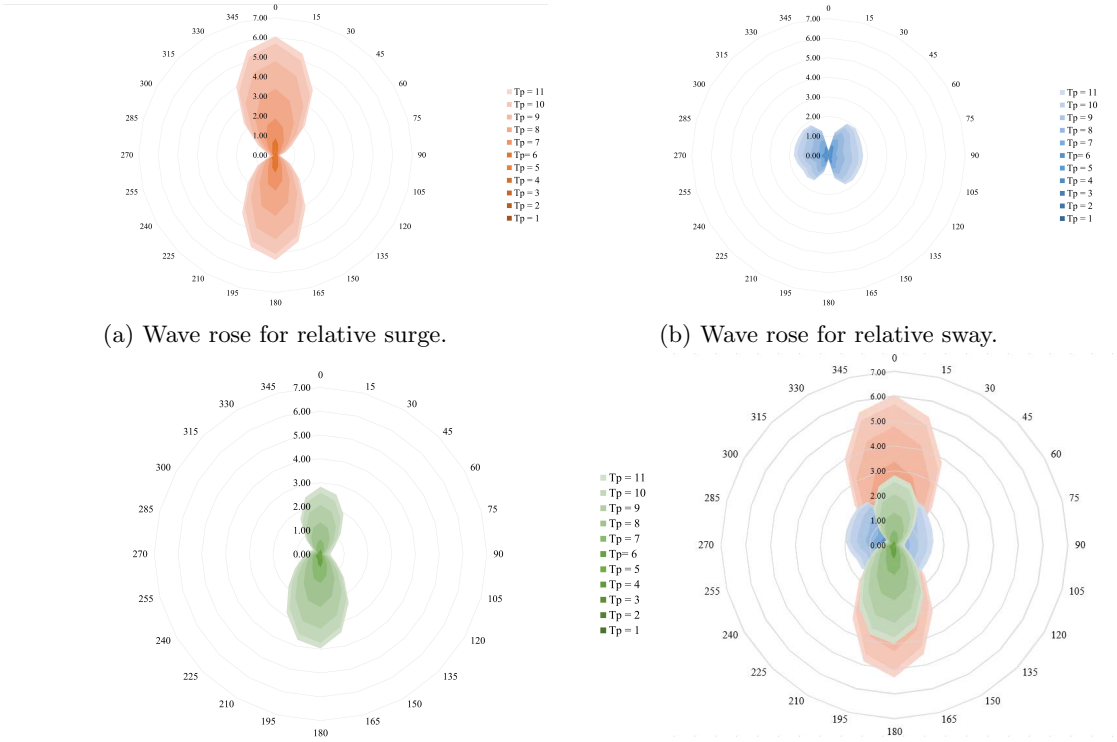

(a) Wave rose for relative surge.

(b) Wave rose for relative sway.

(c) Wave rose for relative heave.

(d) Combined wave rose.

Figure 7.2: Wave directionality in relative surge, sway and heave for a floating-to-floating operation.

Lastly, closer inspection of the wave directions in Figure 7.2d reveals that the optimal wave direction for minimizing the relative motion in surge, sway, and heave is 240° due to the small amplitude of both surge and heave. This wave direction results in the lowest maximum relative displacement compared to other directions. The relative sway is a limiting factor for this wave direction. A favorable range for performing the floating-to-floating operation is found between 45 to 135° and 225 to 315°. As discussed in Chapter 4, the site experiences 92% of all waves from the direction of 90 to 180°. Therefore, selecting the relative position of the operation to coincide with these ranges would minimize the relative motions.

Assuming a wave direction of 240° the optimal conditions for conducting floating-to-floating lift operations can be achieved, resulting in relative motions as shown in Figure 7.3. This leads to a workability rate of 51%, as shown in Figure 7.4, which is a significant 20% improvement over the worst-case scenario as shown in Chapter 6. The above analysis underscores the significance of

factoring in wave directionality when planning on-site marine operations and designing wind farm lay-outs.

		Peak period (s)								
		1 < Tp < 2	2 < Tp < 3	3 < Tp < 4	4 < Tp < 5	5 < Tp < 6	6 < Tp < 7	7 < Tp < 9	9 < Tp < 10	10 < Tp < 11
Significant wave height (m)	Hs < 1	0.00	0.01	0.05	0.12	0.23	0.40	1.02	1.31	1.50
	1 < Hs < 2		0.02	0.09	0.25	0.46	0.80	2.05	2.61	3.00
	2 < Hs < 3			0.13	0.37	0.69	1.20	3.07	3.92	4.50
	3 < Hs < 4				0.49	0.92	1.61	4.09	5.23	6.00
	4 < Hs < 5						2.02	5.09	6.88	7.59
	5 < Hs < 6							6.08	8.58	9.71
	6 < Hs < 7								10.29	11.88
	7 < Hs < 8								11.95	14.09

Figure 7.3: Relative amplitude in sway for a wave direction of 240°.

		Peak period (s)									
		1 < Tp < 2	2 < Tp < 3	3 < Tp < 4	4 < Tp < 5	5 < Tp < 6	6 < Tp < 7	7 < Tp < 9	9 < Tp < 10	Tp > 11	
Significant wave height (m)	Hs < 1	0.03%	4.69%	7.29%	7.02%	3.91%	5.91%	13.49%	6.27%	0.08%	28.85%
	1 < Hs < 2		0.00%	0.92%	6.64%	6.85%	7.32%	7.90%	8.36%	0.16%	21.73%
	2 < Hs < 3			0.00%	0.09%	0.55%	2.71%	2.91%	3.32%	0.15%	0.64%
	3 < Hs < 4				0.00%	0.01%	0.12%	1.11%	1.04%	0.08%	0.01%
	4 < Hs < 5						0.00%	0.19%	0.47%	0.04%	
	5 < Hs < 6							0.02%	0.21%	0.01%	
	6 < Hs < 7								0.08%	0.01%	
	7 < Hs < 8								0.02%	0.01%	
		0.03%	4.69%	8.21%	13.75%	11.32%	13.23%				51.23%

Figure 7.4: Probability distribution in sway for a wave direction of 240°.

7.2 Floating-to-fixed operation

Figure 7.5 compares the wave directionality for motion between the crane tip and a stationary hub to that of the relative motion between the crane tip and a moving hub. The directional characteristics of wave-induced motion for a floating-to-fixed operation are depicted in darker colors, in comparison to those for a floating-to-floating operation, which are represented by lighter colors.

Figure 7.5a presents a comparison of the surge between the two cases. The findings suggest that the wave directionality in surge for the floating-to-fixed operation differs only slightly from that observed in the floating-to-floating operation. A larger heave displacement is noticeable in Figure 7.5b for a wider range of wave directions during the floating-to-fixed operation. However, given that the heave displacement is still relatively minor when compared to the surge and the fact that the relative motion criterion for heave is larger, it is not a limiting factor in selecting the optimal wave direction for the floating-to-fixed operation.

One of the most favorable wave directions for the floating-to-fixed operation is 150°, which yields a workability rate of 51%.

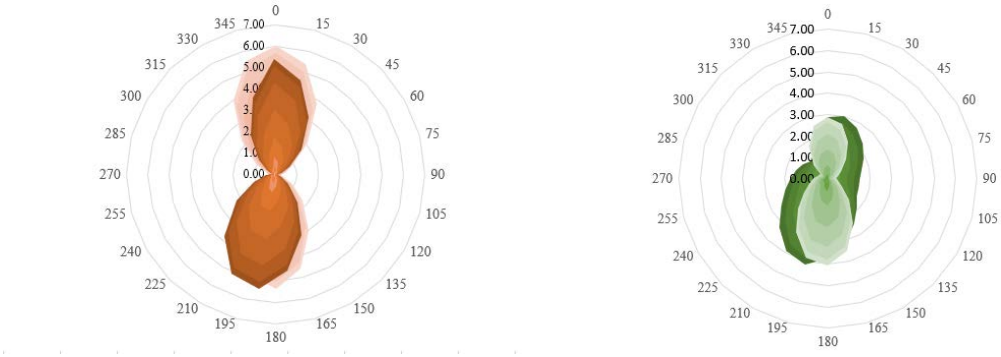

(a) Wave rose for relative surge.

(b) Wave rose for relative heave.

Figure 7.5: Wave directionality comparison between the relative motion of a floating-to-fixed (dark colors) and a floating-to-floating (lighter colors) operation.

To summarize, the sensitivity study reveals that the wave direction significantly influences the workability of the floating-to-floating and floating-to-fixed operation. Finally, slight differences in wave directionality between the floating-to-floating and floating-to-fixed operations are observed.

Chapter 8

Alternative solution

This chapter aims to investigate alternative solutions for installing a 15MW blade on a floating offshore wind turbine. Structurally connecting the turbine to the vessel allows them to move together in response to the wave forces. Section 8.1 offers a brief overview of the solutions for fixed-to-fixed operations available in the offshore industry, while Section 8.2 does so for floating-to-floating solutions.

8.1 Fixed-to-fixed solutions

8.1.1 Sjøhest Wind Blade Installation

An alternative solution for fixed-to-fixed blade installation was presented in 2022 by GustoMSC. The Sjøhest Wind Blade Installation (WBI) solution involves the use of a fixed vessel, such as a jack-up and is visualized in Figure 8.1 [46]. The procedure involves positioning the Sjøhest in front of the tower using a cantilever that can move horizontally in two directions, along both the x and y axes. The Sjøhest is connected to the already-installed tower using a telescopic leader boom that passively aligns with the tower's movements to create an aligned movement between the blade and the tower. The tower is connected using a gentle tower gripper that disallows sliding or rolling and does not use heave compensation. A smaller handling crane picks up the blade with a blade handling tool and docks the tool and blade as one package onto the trolley. The blade is horizontally transported up along the leader boom, rotated into a vertical position, and connected to the hub. Afterwards, the hub is rotated and the next blade is installed in a similar matter. Figure 8.1 shows the different steps in the operation.

The benefits of the system are:

1. The WBI has passive alignment with tower motions. The gripper is moving together with the tower, excluding the need for heave compensation.
2. The soft gripper on the tower ensures no sliding and no rolling.
3. Gripping the blade only once reduces the risk of damage.
4. WBI saves 20-30% of schedule time compared to using a single large jack-up for all motions.
5. The WBI can operate under wind speeds up to 17/18 m/s, compared to wind speeds up to 10 m/s for single blade installation.
6. The blade gripped by the blade handling tool, thus firmly supported in stead of hanging from a crane hook.

The primary obstacle in implementing this system for a floating-to-floating solution is that passive alignment, which works well for fixed-to-fixed installations where relative motions are minimal, may not be effective in this scenario. Due to the potential for large differences in motion between the two bodies, excessive loads may be transferred to the structure, potentially compromising its structural integrity.

Figure 8.1: Sjøhest Wind Blade Installation Solution by GustoMSC [46].

8.2 Floating-to-fixed solutions

8.2.1 Blade Installation Tool

In 2016, Temporary Works Design (TWD) and Royal Wagenborg (RW) implemented a Blade Installation Tool (BIT) that employs a similar strategy, only now for a floating-to-fixed blade installation [47]. During the initial engagement phase, the BIT approaches the turbine tower. The boom comprises two sections: the bottom boom, which is hinged to the floating vessel at an angle, and the top boom, which is aligned and connected to the tower at two points. Tugger lines are attached to the bottom crane boom and utilized to prevent large horizontal forces from being exerted on the tower. The blade is picked up by the blade manipulator and transported horizontally up the bottom boom using the bottom blade handling cart. The top boom is equipped with another blade handling cart. The blade manipulator travels from the bottom cart to the top cart, after which the blade is rotated and vertically connected to the hub. The BIT then travels down the boom, the hub is rotated, and the process begins anew for the subsequent blade. Figure 8.2 displays the operation steps. This system utilizes active motion compensation in heave, pitch and roll to compensate the motions of the floating vessel when approaches the turbine. Once connected to the tower, a switch to passive motion compensation as the fixed turbine tower acts as a stability reference point. The passive alignment works with a hinged BIT and the up and down sliding of the bottom boom on the top crane boom.

The benefits of the system are:

1. The blade manipulator grips the blade, providing firm support, as opposed to suspending it from a crane hook.
2. The alternative blade installation method is effective at higher wind speeds compared to conventional blade installation.
3. A heavy transport vessel, a barge and platform supply vessel can be equipped with the BIT.

The research and design project on the BIT, which received funding from the Dutch government, identified the primary challenges as follows: the motion-compensated gripping of the tower during the "Engaging phase", holding and tracking the tower during the "Engaged phase", and lifting the blade and inserting it into the nacelle during the "Blade lifting phase." Nevertheless, the implementation of the Blade Exchanger for a floating-to-floating solution poses an additional challenge due to the lack of a static reference point, as the floating wind turbine also experiences motion. The tower tracking process is anticipated to be more challenging, with particular difficulty expected during the transition from the bottom boom to the slider on the top boom. The hinge and heave slider present in the system may not be sufficient to compensate for the relative movements. Additionally, it should be noted that the BIT is only designed for 5 MW turbine blades, which may limit its applicability for larger turbines.

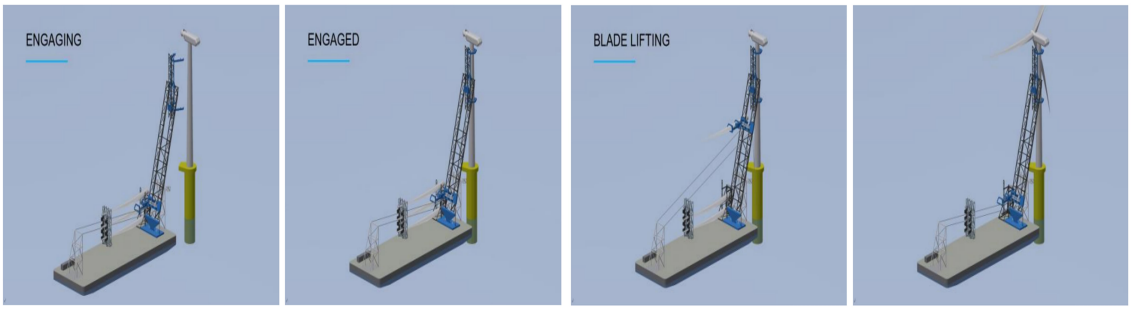

Figure 8.2: Blade Installation Tool by TWD and RW [47].

8.2.2 Blade Exchanger

The Blade Exchanger, developed by a consortium consisting of Barge Master and TWD, is a system designed for the installation of blades with a floating-to-fixed operation [48]. The system operates by aligning the floating vessel with the wind turbine in a stern-to-hub orientation. A telescopic crane is then utilized to lift the blades from the blade rack, expand and rotate them in the air, and connect them vertically to the hub. To counteract the relative motion between the fixed floating vessel and the wind turbine, the telescopic crane is equipped with a 3D motion-compensated Barge Master Platform, which can compensate for roll, pitch, and heave. This ensures that the system operates effectively, eliminating any potential interference caused by the movement of the floating vessel. Vessel motion in surge, sway and yaw is accounted for by the DP and mooring system.

The benefits of the system are:

1. The system does not require large deck space, therefore more blades can be stacked on deck.
2. The system is vessel independent.
3. The system eliminates the need to reach over the top of the nacelle.

The primary obstacle in implementing the Blade Exchanger for a floating-to-floating solution is again the motion of the floating wind turbine, as the two bodies are not structurally linked. Even if the blade is vertically attached, the mating process still occurs at a significant height. Furthermore, a stand-alone crane is responsible for rotating the blade mid-air from a horizontal to a vertical position. The possibilities for structurally linking the floating wind turbine to the crane vessel are limited due to the blade dimensions, which prevent any connection near the mating point. Also, multiple motion compensation systems are expected to be necessary. This raises questions about the benefits of using this approach compared to the standard single blade installation procedure.

Figure 8.3: Blade Exchanger by Barge Master and TWD [48].

To summarize, the process of physically linking the Tri-floater and installation vessel poses several challenges and a solution to these challenges has not yet been found.

Chapter 9

Conclusion

The aim of this research was to investigate the operational feasibility of on-site installation of a 15 MW wind turbine blade on a semi-submersible floating wind turbine using a floating crane vessel, to analyse the factors which impact the operational feasibility and to compare it to that the on-site blade installation of bottom-fixed wind turbines.

In this thesis, the operational feasibility is determined by a workability assessment. The installation procedure focuses on the critical phase of single blade installation, specifically the mating phase between the blade root and the hub. A set of relative motion criteria were developed based on the compensation strokes in x-, y- and z- direction to establish the operational limits for the relative motion between the crane tip and the hub. A schematic overview of the relative translations is shown in Figure 9.1. A simplified frequency-domain multi-body model was used to determine the motion RAOs of the Tri-floater and the crane vessel, and the subsequent the relative motion RAO. The model assumed first order potential flow, rigid body motions for the Tri-floater and the crane vessel, and neglected wind and current loads. The JONSWAP wave spectrum and motion spectrum were used to obtain the response spectrum, from which the MPM values were calculated to determine the workability. To establish a benchmark for the workability of floating-to-floating installation, workability calculations were also performed for blade installation of bottom-fixed wind turbines. On-site blade installation for bottom-fixed wind turbines is divided into two operations: floating-to-fixed, where the Tri-floater is replaced with a stationary point, and fixed-to-fixed, which applies the generally accepted environmental limit of a significant wave height of 2 m. The workability calculations are performed using a scatter diagram of a site with moderate wave conditions, located in the Gulf of Maine, USA.

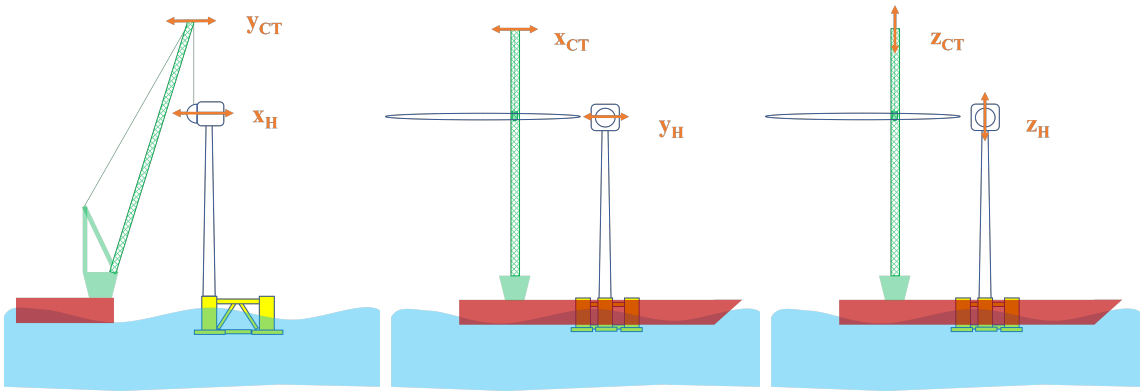

(a) Hub and crane tip translations in global surge. (b) Hub and crane tip translations in global sway. (c) Hub and crane tip translations in global heave.

Figure 9.1: Schematic overview of the relative translations.

First of all, the multi-body model analysis revealed that the presence of the crane vessel has a

noticeable impact on the motion of the Tri-floater, as confirmed by comparing its motion with that predicted by the single-body model. It is evident that the motion response is reduced when the crane vessel is able to shield the Tri-floater from incoming waves. Conversely, if the incoming waves first approach the Tri-floater, the reflected waves from the crane vessel impact the motion of the Tri-floater. The effect of the Tri-floater's presence on the crane vessel motion is much smaller. The crane vessel did not experience any benefit from the shielding effect. This discrepancy could be attributed to the Tri-floater's braced structure which makes it permeable to waves. Instead of shielding the crane vessel, the Tri-floater's cylindrical structure causes waves to diffract in multiple directions. One of the questions emerging from this finding relates specifically to the size of the crane vessel. A relatively large monohull crane vessel is selected for this study, while a smaller and more cost-effective crane vessel is probably required to enable successful implementation of on-site floating wind turbine installation.

Second of all, it can be concluded that the workability of the on-site 15 MW blade installation on the Tri-floater using a crane vessel ranges from 31% to 51%. The variation in workability attributed to the wave directionality. The relative surge between the crane tip and the hub is limiting for the floating-to-floating installation. The results of this research indicate that the roll motion of the crane vessel has a significant impact on the relative motions at large installation height. The workability of a fixed-to-fixed operation is 87%.

Contrary to expectations, this study did not find a significant difference between the workability of the floating-to-floating operation to that of the floating-to-fixed operation. It could be argued that the crane vessel is more influential on the relative motion of the operation than the Tri-floater. Despite the Tri-floater's design to avoid natural periods overlapping with wave periods, more significant discrepancies between the two were expected. While there are some slight differences in wave directionality between the floating-to-floating and floating-to-fixed operations, they are not significant. While introducing the wind turbine poses its own set of challenges, it is not considered the most difficult step. The greatest challenge lies in transitioning from fixed-to-fixed to floating-to-fixed blade installations, as the crane vessel is responsible for the largest motions.

Moreover a sensitivity study was performed and showed that the wave direction has significant impact on the relative motion and the workability. The observed optimal orientation was 240°, resulting the upper workability of 51%. The relative surge and relative heave are reduced to a minimum, resulting in the relative motion limit being reached primarily in the relative sway direction. The critical wave direction is 0°, resulting in the lower workability limit of 31%.

In conclusion, the findings of this study indicate that the workability of a floating-to-floating single blade installation is approximately half of that of a fixed-to-fixed installation. Alternative solutions for single blade installation, such as the Sjøhest, BIT, or Blade Exchanger, show potential to address the challenges associated with involving at least one floating component, however these solutions are not yet suitable for floating-to-floating operations and some are still in early phase of development. This highlights the need for further advancements to fully unlock the vast potential of the floating wind industry.

Chapter 10

Discussion and recommendations

This chapter discusses the limitations and corresponding recommendations for further research.

This research neglects environmental loads such as current and wind loads which could influence the operation and cause variations in the workability. Neglecting the effects of current loads may result in overestimating the workability of the operation, particularly if the site is located in an area with strong currents. For an operation with a short time frame, the influence of current loads may be relatively small compared to the impact of other environmental factors. Neglecting the effects of wind loads, particularly at greater operational heights, can have significant impacts on the performance and safety of the operation. The pendulum motion of the blade hanging under the crane hook is not taken into account into this research, which could be significantly impacted by wind loads. To accurately assess the workability of a floating-to-floating single blade installation, it is advisable to incorporate wind loads and linear frequency wind-induced motion into the model.

The workability of a floating-to-floating single blade installation is approximately half of that of a fixed-to-fixed installation, when only considering waves. One area of focus for future research could be exploring the structural connection between the Tri-floater and crane vessel. This research could lead to the development of innovative methods to securely and efficiently connect the two structures, potentially improving the overall workability of the installation procedure.

Various hydrodynamic interaction phenomena, such as the shielding effect, occur during a floating-to-floating wind turbine installation, such as the shielding effect caused by the crane vessel. Research should focus on investigating the influence of the vessel's size on this effect, and its subsequent impact on the relative motion between the two structures.

The research uses a frequency domain model to calculate the hydrodynamic coefficients, added mass, radiation damping, and wave forces of the Tri-Floater and crane vessel. This means only linear equations are used. The non-linear wave effects, including second-order wave loads and wave drift forces, are disregarded as they are not very relevant for the relatively small sea states during installation. Additionally, it is assumed that the cane vessel will maintain its position and heading. It is assumed that the crane and tower are rigid and, therefore, no deformation takes place. However, with the expected increase in wind turbine size, the deformation and flexibility on the crane and tower could become more significant. Including these non-linear effects is recommended as wind turbines increase even more in size. Tagline dynamics are commonly acknowledged to be nonlinear due to the non-linear correlation between the displacement of the vessel and the tension in the lines. Hence, it is advisable to incorporate these effects while constructing a time-domain non-linear model.

While this study assumes that the Tri-floater is freely floating, the stiffness of the mooring lines can have a significant impact on the natural frequency of the Tri-floater and its position. It is therefore recommended to investigate the effect of the mooring line stiffness on the relative motion.

The workability calculations are only performed for a fixed horizontal gap distance of 61 m. In a further extended study, more distances could be analysed. It is advised to investigate the possibility of resonance gap behavior between the Tri-floater and crane vessel, occurring when the wavelength is comparable to the horizontal distance. It could be quite relevant to check from

what distance between the Tri-floater and crane vessel the resonance gap behavior can occur, especially to establish the boundary conditions of the operation. This is especially recommended for smaller horizontal gap distances. The research conducted by N. van Duijn [49] indicates that resonance behavior has minimal effects on workability when calculating a lift between two semi-submersible vessels with a gap distance of 40 m. However, further validation is advised to confirm that resonance gap behavior does not affect the workability of an operation with a floating wind turbine and a crane vessel.

In conclusion, this preliminary research has raised several questions that require further investigation. To comprehensively understand the variation in workability between floating-to-fixed and floating-to-floating installations, additional research is recommended, which should include wind loads and blade pendulum motion. Another area for further research could be the development of a specialized blade installation tool, which could accelerate successful on-site installation of floating wind turbines.

Bibliography

[1] IEA. Net Zero by 2050 - A Roadmap for the Global Energy Sector. Technical report, 2021. URL www.iea.org/t&c/.

[2] Fiona Harvey, Jillian Ambrose, and Patrick Greenfield. More than 40 countries agree to phase out coal-fired power, 11 2021. URL https://www.theguardian.com/environment/2021/nov/03/more-than-40-countries-agree-to-phase-out-coal-fired-power.

[3] IRENA. World Energy Transitions Outlook 1.5° C Pathway. Technical report, Abu Dahbi, 2021. URL www.irena.org.

[4] GWEC. Global Offshore Wind Report 2021. Technical report, Global Wind Energy Council, Brussels, Belgium, 9 2021. URL www.gwec.net.

[5] The Carbon Trust. Floating Wind Joint Industry Project: Phase II Summary Report. Technical report, 6 2020.

[6] International Energy Agency. Offshore Wind Outlook 2019: World Energy Outlook Special Report. Technical report, 11 2019. URL www.iea.org/t&c/.

[7] Zi Lin, Xiaolei Liu, and Saeid Lotfian. Impacts of water depth increase on offshore floating wind turbine dynamics. *Ocean Engineering*, 224:108697, 3 2021. ISSN 0029-8018. doi: 10.1016/J.OCEANENG.2021.108697.

[8] Offshore Magazine. Hywind Scotland sets UK wind farm capacity record, 3 2021. URL https://www.offshore-mag.com/renewable-energy/article/14199938/hywind-scotland-sets-uk-offshore-wind-farm-capacity-record.

[9] The Carbon Trust. Floating Wind Joint Industry Project Phase III Summary Report. Technical report, 2021. URL www.carrenoir.com.

[10] Adrijana Buljan. Scotland's New Floating Wind Projects – What We Know So Far. *OffshoreWind.biz*, 1 2022. URL https://www.offshorewind.biz/2022/01/18/scotlands-new-floating-wind-projects-what-we-know-so-far/.

[11] WindEurope. Floating Offshore Wind Vision Statement. Technical report, 2017.

[12] WindEurope. Ports: a key enabler for the floating offshore wind sector. 9 2020.

[13] Isabelle Van Der Kaaij. Installation and Maintenance for the Next Generation of Floating Offshore Wind Turbines: a Technical Review. Technical report, 2022.

[14] DNV. DNVGL-ST-0119 Floating wind turbine structures. Technical report, 2018. URL http://www.dnvgl.com,.

[15] DNV. DNV-OS-H101 Marine Operations, General. Technical report, 2011. URL http://www.dnv.com.

[16] DNV. DNVGL-ST-0378 Standard for offshore and platform lifting appliances. Technical report, 2016. URL http://www.dnvgl.com,.

[17] Sarah Killoh. Heerema installs first wind turbine using novel RNA method, 11 2022. URL https://www.heerema.com/news/heerema-installs-first-wind-turbine-using-novel-rna-method.

[18] Equinor. How Hywind works. URL https://www.equinor.com/en/what-we-do/floating-wind/how-hywind-works.html.

[19] Rahul Chitteth Ramachandran, Cian Desmond, Frances Judge, Jorrit-Jan Serraris, and Jimmy Murphy. Floating offshore wind turbines: Installation, operation, maintenance and decommissioning challenges and opportunities. *Wind Energy Science Discussions*, pages 1–32, 2021. ISSN 2366-7443. doi: 10.5194/wes-2021-120.

[20] Scaldis. Transport and Installation of two 5MW Wind Turbine Generators for the Beatrice Demonstrator Project. URL http://www.scaldis-smc.com/en/projects/groen-2007-jul-beatrice/.

[21] Project Cargo Journal. Boskalis: Kincardine is a prelude to more floating wind projects, 2 2021. URL https://www.projectcargojournal.com/offshore/2021/02/18/boskalis-kincardine-is-a-prelude-to-more-floating-wind-projects/.

[22] Dang Ahn, Sung Chul Shin, Soo Young Kim, Hicham Kharoufi, and Hyun Cheol Kim. Comparative evaluation of different offshore wind turbine installation vessels for Korean west–south wind farm. *International Journal of Naval Architecture and Ocean Engineering*, 9(1):45–54, 1 2017. ISSN 2092-6782. doi: 10.1016/J.IJNAOE.2016.07.004.

[23] Zhiyu Jiang. Installation of offshore wind turbines: A technical review. *Renewable and Sustainable Energy Reviews*, 139, 4 2021. ISSN 1364-0321. doi: 10.1016/J.RSER.2020.110576.

[24] Amrit Shankar Verma, Zhiyu Jiang, Nils Petter Vedvik, Zhen Gao, and Zhengru Ren. Impact assessment of a wind turbine blade root during an offshore mating process. *Engineering Structures*, 180:205–222, 2 2019. ISSN 18737323. doi: 10.1016/j.engstruct.2018.11.012.

[25] Ron Voerman. Horizontal single blade mounting tool for offshore wind turbine installation. URL https://www.macartney.com/what-we-offer/cases/horizontal-single-blade-mounting-tool-for-offshore-wind-turbine-installation/.

[26] F Sevilla, R Redfern, A Storey, N Baldock, and P Dutton. Optimization of Installation, Operation and Maintenance at Offshore Wind Projects in the U.S.: Review and Modeling of Existing and Emerging Approaches. Technical report, 2014.

[27] Saipem. Hywind. URL https://www.saipem.com/en/projects/hywind.

[28] Diane Pham. The WindFlip Barge Concept Installs Offshore Wind Turbines Inexpensively and With Ease, 12 2011. URL https://inhabitat.com/the-windflip-barge-concept-installs-offshore-wind-turbines-inexpensively-and-with-ease/.

[29] Ulstein. WINNER OF STATOIL CHALLENGE, 8 2015. URL https://ulstein.com/news/winner-of-statoil-challenge.

[30] Zhiyu Jiang, Lin Li, Zhen Gao, Karl Henning Halse, and Peter Christian Sandvik. Dynamic response analysis of a catamaran installation vessel during the positioning of a wind turbine assembly onto a spar foundation. *Marine Structures*, 61:1–24, 9 2018. ISSN 0951-8339. doi: 10.1016/J.MARSTRUC.2018.04.010.

[31] Zhiyu Jiang, Rune Yttervik, Zhen Gao, and Peter Christian Sandvik. Design, modelling, and analysis of a large floating dock for spar floating wind turbine installation. *Marine Structures*, 72, 7 2020. ISSN 09518339. doi: 10.1016/j.marstruc.2020.102781.

[32] Liftra. LT975 - Blade Dragon. URL https://www.liftra.com/products/lt975-blade-dragon.html.

[33] Zhiyu Jiang, Zhen Gao, Zhengru Ren, Ye Li, and Lei Duan. A parametric study on the final blade installation process for monopile wind turbines under rough environmental conditions. *Engineering Structures*, 172:1042–1056, 10 2018. ISSN 0141-0296. doi: 10.1016/J.ENGSTRUCT.2018.04.078.

[34] A L Slootweg. Single blade installation with a floating monohull vessel: Establishing the operational limits while using dynamic controlled taglines. Technical report.

[35] Evan Gaertner, Jennifer Rinker, Latha Sethuraman, Frederik Zahle, Benjamin Anderson, Garrett Barter, Nikhar Abbas, Fanzhong Meng, Pietro Bortolotti, Witold Skrzypinski, George

Scott, Roland Feil, Henrik Bredmose, Katherine Dykes, Matt Shields, Christopher Allen, and Anthony Viselli. Definition of the IEA Wind 15-Megawatt Offshore Reference Wind Turbine Technical Report. Technical report, 2020. URL www.nrel.gov/publications.

[36] Fons Huijs, Ebert Vlasveld, Maël Gormand, Feike Savenije, Marco Caboni, Bruce Leblanc, Carlos Simao Ferreira, Koert Lindenburg, Sébastien Gueydon, William Otto, and Benoît Paillard. Integrated design of a semi-submersible floating vertical axis wind turbine (VAWT) with active blade pitch control. In *Journal of Physics: Conference Series*, volume 1104. Institute of Physics Publishing, 11 2018. doi: 10.1088/1742-6596/1104/1/012022.

[37] DNV completes Concept Certification and Technical & Commercial assessments of GustoMSC's Tri-Floater, 12 2021. URL https://www.nov.com/about/news/dnv-completes-successful-reviews-of-gustomsc-tri-floater.

[38] GustoMSC. Tri-Floater Floating Offshore Wind Turbine Foundation Brochure. Technical report, 2021.

[39] GustoMSC. GustoMSC introduces the ENSIS next-generation heavy lift crane vessel series, 2022. URL https://www.nov.com/about/news/gustomsc-introduces-the-ensis-next-generation-heavy-lift-crane-vessel-series.

[40] Asgeir J Sørensen. Marine Cybernetics Towards Autonomous Marine Operations and Systems Lecture Notes. Technical report, 2018. URL http://folk.ntnu.no/assor/.

[41] DNVGL. Qualification of innovative floating substructures for 10MW wind turbines and water depths greater than 50m. Technical report, 2015.

[42] Wilson Ivan Guachamin Acero. *Assessment of marine operations for offshore wind turbine installation with emphasis on response-based operational limits*. PhD thesis, Norwegian University of Science and Technology, Trondheim, 12 2016.

[43] Henrik Bredmose. 46211 Offshore Wind Energy, 8 2020.

[44] K. de Leeuw. *Single lift blade alignment for large offshore wind turbines*. PhD thesis, 12 2019.

[45] Cranemaster. Passive Heave Compensators, 2023. URL https://cranemaster.com/products/passive-heave-compensators/.

[46] GustoMSC. Sjohest Blade Installation, 2022. URL https://www.nov.com/products/sjohest-blade-installation.

[47] Blade Installation Tool - Openbaar Eindrapport - Wind op Zee - R&D Projecten. Technical report, Temporary Works Design, Royal Waenborg, 6 2020. URL https://projecten.topsectorenergie.nl/storage/app/uploads/public/613/601/160/613601160a740257523522.pdf.

[48] Barge Master. Blade Exchanger. URL https://www.barge-master.com/fileadmin/user_upload/Documenten/PDF/BM-T700_Motion_Compensation_Platform/BM-MA-FL-4009-Rev0_Barge_Master_-_Blade_Exchanger_spec_sheet.pdf.

[49] Niels Van Duijn. *QUAD lift Workability Analysis: Evaluating the Dynamic Interaction Between Two Dualcrane Vessels using a Frequency Domain Modelling Technique*. PhD thesis, Delft University of Technology, 11 2020.

[50] Denis Matha, Frank Lemmer, and Michael Muskulus. Offshore turbines with bottom-fixed or floating substructures. In *Wind Energy Modeling and Simulation - Volume 2: Turbine and System*, pages 125–167. Institution of Engineering and Technology, 12 2019. doi: 10.1049/pbpo125g{_}ch5.

[51] Odd Magnus Faltinsen. Sea Loads on Ships and Offshore Structures. *Cambridge University Press*, 1993.

[52] J M J Journée and W W Massie. Offshore Hydromechanics. Technical report, 2001.

[53] Subrata K Chakrabarti. Handbook of Offshore Engineering. Technical report, 2005. URL http://elsevier.comllocate/permissions,.

[54] Leo H. Holthuijsen. *Waves in Oceanic and Coastal waters*. Cambridge University Press, 2 2010. ISBN 9780511618536. doi: https://doi-org.tudelft.idm.oclc.org/10.1017/CBO9780511618536.

Appendix A: Waves

The main goal of this chapter is to offer a comprehension of hydrodynamics, with a specific focus on linear potential flow theory and linear wave loads. Although higher-order theories will also be briefly discussed, the primary emphasis will be on linear theories. Additionally, the wave spectrum will be described towards the end of the chapter.

Hydrodynamics

The present study employs potential flow theory for a frequency domain hydrodynamic analysis. However, it should be noted that potential flow theory has its limitations, as it disregards significant physical phenomena like viscosity, turbulence, and the influence of boundary layers.

Potential flow

Potential flow theory is a fundamental fluid mechanics theory widely described in literature. The velocity potential ϕ is introduced to describe the fluid velocity vector $\mathbf{V}$, dependent on both space and time.

A freely floating body with zero mean forward speed is considered. The linear wave velocity potential is defined as:

$$\phi(x, y, z, t) = \phi_r(x, y, z, t) + \phi_w(x, y, z, t) + \phi_d(x, y, z, t) \tag{10.1}$$

In this context, the radiation potential is denoted as ϕ_r, the incident wave potential as ϕ_w, and the diffraction potential as ϕ_d. This research refers to the function $\phi(x, y, z, t)$ as simply ϕ from now on. The velocity of the fluid at any point in the flow is obtain by taking the gradient of the velocity potential.

$$\mathbf{V} = \nabla\phi \equiv \mathbf{i}\frac{\partial\phi}{\partial x} + \mathbf{j}\frac{\partial\phi}{\partial y} + \mathbf{k}\frac{\partial\phi}{\partial z} \tag{10.2}$$

The assumption is made that the fluid is both inviscid and irrotational. To save computational cost and time, it is a typical engineering practice to solve the Laplace equation for potential flow instead of the full Navier-Stokes equations, as stated by Matha (2019) [50]. If the flow is assumed to be incompressible, the Laplace equation is satisfied by the velocity potential.

$$-\nabla^2\phi = 0 \tag{10.3}$$

The Bernoulli equation establishes the connection between fluid pressure p and ϕ.

$$p + \rho g z + \rho\frac{\partial\phi}{\partial t} + \frac{\rho}{2}\mathbf{V}\cdot\mathbf{V} = C \tag{10.4}$$

The equation involves various parameters, including ρ, which represents the fluid density, ν denoting the kinematic viscosity, g representing the gravitational constant, z indicating the height of the water column measured from the sea bottom (where z equals zero at the sea bottom) and

increasing positively upwards, and C, which is the integration constant. The kinematic boundary condition is established by assuming that the sea bottom is impermeable.

$$\frac{\partial \phi}{\partial n} = 0 \quad \text{on the sea bottom} \tag{10.5}$$

Here, $\frac{\partial \phi}{\partial n}$ represents differentiation along the normal direction. In the case of a body in motion, the kinematic boundary condition can be expressed as follows:

$$\frac{\partial \phi}{\partial n} = \mathbf{U_b} \cdot \mathbf{n} \quad \text{on the body surface} \tag{10.6}$$

In the above equation, $\mathbf{U_b}$ denotes the velocity of the body in motion. Additionally, the dynamic free-surface condition stipulates that the water pressure on the free surface is equal to a constant atmospheric pressure. For further theoretical background, the work of [51] is recommended. By linearizing and combining the free-surface conditions, the interaction between linear waves and linear wave-induced motions can be investigated.

$$\frac{\partial^2 \phi}{\partial t^2} + g\frac{\partial \phi}{\partial z} = 0 \quad \text{on} \quad z = 0 \tag{10.7}$$

These equations form the foundation for selecting wave theory and solving fluid-structure interaction problems.

Wave theories

The particle kinematics of a wave field can be described by many different wave theories with varying levels of complexity. Wave kinematics include particle velocities and accelerations. Literature studied for this chapter include the books Offshore Hydrodynamics by Journée and Massie [52], The Handbook of Offshore Engineering by Chakrabarti [53] and Sea Loads on Ships and Offshore Structures by Faltinson [51].

In offshore engineering, there are various wave theories that can be employed, depending on the specific values of wave height H, wave period T, and water depth h. The selection of an appropriate wave theory is determined by these three parameters. Le Méhauté proposed a wave diagram, shown in Figure 10.1, which illustrates the range of validity of different finite amplitude wave theories as a function of these parameters.

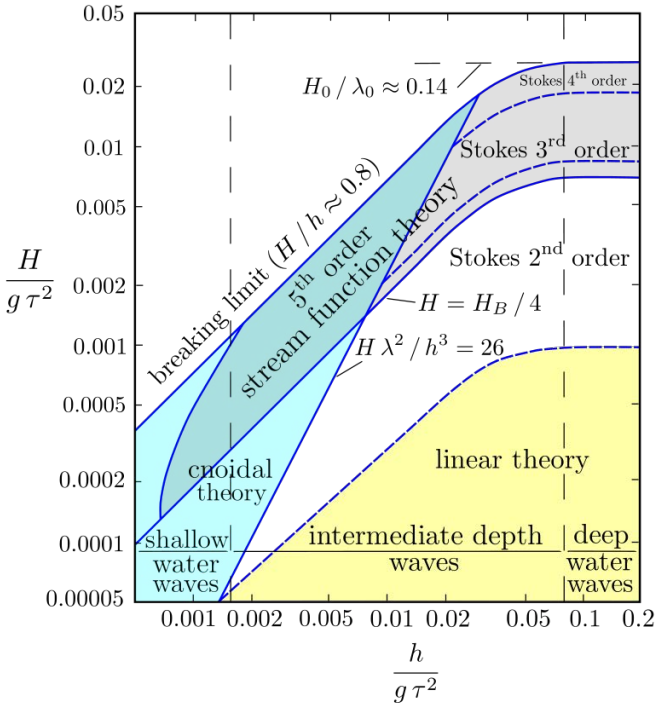

Figure 10.1: Comparison of different wave theories as a function of wave height, water depth and wave period [43]

The ratio of water depth to the wavelength, λ, is an important parameter for determining whether a wave is a shallow, intermediate, or deep water wave. The cnoidal, stream function, and breaking limit wave theories are mainly used for shallow water waves. Only wave theories suitable for deep water waves will be discussed in this research, as they are relevant for floating wind farm sites. If $h \geq \frac{\lambda}{2}$, the wave can be considered a deep water wave, indicating that the wave characteristics are not significantly affected by the seafloor.

Linear Wave Theory

Linear wave theory, also known as Airy wave theory, is a simplified method that describes the motion of a regular sinusoidal wave in two dimensions. This theory provides reasonable approximations of wave characteristics, although its applicability is limited. It assumes that the wave amplitude is small and the water depth is constant. A wave can be described as a regular wave, a wave with a constant and uniform wave shape, meaning that the wave profile repeats itself exactly over time.

The Laplace equation, discussed in 10, is solved with linearized boundary conditions, assuming small amplitude waves in linear wave theory where higher order terms are neglected. An analytical solution of the Laplace equation is a long-crested harmonic wave that propagates in the positive x-direction [54]. The free surface elevation, dependent on both time (t) and space (x) is denoted:

$$\eta(x,t) = Asin(\omega t - kx) \tag{10.8}$$

In the above equation, A is the wave amplitude, ω the wave frequency which is equal to $\frac{2\pi}{T}$ and k the wave number. The frequency is related to the wave number and water depth via the dispersion relation:

$$\omega^2 = kgtanh(kh) \tag{10.9}$$

It should be noted that ocean waves are irregular and can be described as a sum of many regular waves. For irregular waves composed of j regular waves, the free surface elevation can be expressed as:

$$\eta(t,x) = \sum_{j=1}^{N} A_j \sin\left(\omega_j t - k_j x + \epsilon_j\right) \tag{10.10}$$

With the following velocity potential:

$$\phi = \sum_{j=1}^{N} -A_j \frac{\omega_j}{k_j} \frac{\cosh k_j(z+h)}{\sinh k_j h} \sin\left(\omega_j t - k_j x + \epsilon_j\right) \tag{10.11}$$

In the above equation, ϵ_j denotes the random phase angle which is uniformly distributed in the range from 0 to 2 π. The vertical coordinate z is zero at the SWL and negative inside the water column [50].

As long as the the surface wave is harmonic, the horizontal velocity in x-direction u_x and vertical velocity u_z are obtained from the velocity potential. The velocity components are the spatial derivatives of ϕ.

$$u_x = \sum_{j=1}^{N} A_j \omega_j \frac{\cosh k_j(z+h)}{\sinh k_j h} \sin\left(\omega_j t - k_j x + \epsilon_j\right) \tag{10.12}$$

$$u_z = \sum_{j=1}^{N} -A_j \omega_j \frac{\sinh k_j(z+h)}{\sinh k_j h} \cos\left(\omega_j t - k_j x + \epsilon_j\right) \tag{10.13}$$

The y-velocity component is zero because the long-crested harmonic wave propagates only in the positive x-direction.

As shown in Figure 10.2, wave particles in deep water follow nearly circular paths. The velocity induced by the wave decreases exponentially with distance from the surface. The particle motion is harmonic, smooth, and somewhat predictable. A regular deep-water wave generates a more uniform wave force than a wave in intermediate or shallow water, which takes on a more sinusoidal shape.

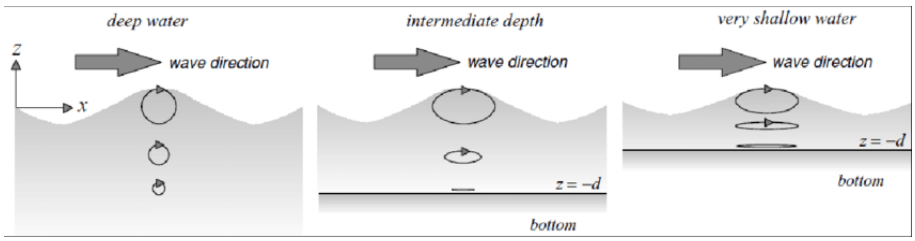

Figure 10.2: Comparison of wave shape for deep water waves, breaking waves and shallow waves [54]

Higher-order wave theories

When the assumptions of linear wave theory are not valid, for example when waves are too steep or the water is too shallow, different wave theories are necessary. Higher-order models have been developed to yield better mathematical approximations of ocean waves. The waves are non-linear, hence superposition to create irregular waves is not an option. The small amplitude assumption expires, it is only assumed that waves have finite amplitude. The wave profile is different compared to sinusoidal waves: a steeper, more peaked crest and a shallow and broad trough. Moreover the crests have higher amplitudes then the troughs. Stokes second-order wave theory uses first-order

components at the wave frequency and second order components at twice the wave frequency. In deeper waters, the contribution of second-order terms is smaller and linear wave theory may be better used [53]. Moreover higher order wave components becomes less important in deep waters. Including higher-order terms may also be relevant for structures with an eigenfrequency close to the high frequencies from these terms. Non-linear wave theories are not further evaluated in this research.

Wave loads

To obtain the linear wave loads on a structure, the hydrodynamic pressure is integrated over the wetted surface of the structure. The hydrodynamic pressure is computed from the velocity potential with the Bernoulli equation as described in Section 10.

$$\mathbf{F} = -\iint_S (p \cdot \mathbf{n}_j) \cdot dS \tag{10.14}$$

The wetted body surface is denoted as S and $\mathbf{n}_j$ as the outward normal vector. The forces and moments are dependent on $\mathbf{n}_j$ and $\mathbf{r}$, the position vector of the surface dS with respect to the origin of the reference frame of the body.

$$\mathbf{n}_j = \begin{cases} \mathbf{n} & \text{for j} = 1, 2, 3 \\ \mathbf{n} \times \mathbf{r} & \text{for j} = 4, 5, 6 \end{cases} \tag{10.15}$$

The forces and moments that arise from various sources include those from radiated waves due to an oscillating body, those from approaching waves on a fixed floating body, those from diffraction of waves caused by a fixed floating body, and those from hydrostatic buoyancy.

$$\mathbf{F}_r = \rho \iint_S \left(\frac{\partial \Phi_r}{\partial t} \right) \mathbf{n}_j \cdot dS \tag{10.16}$$

$$\mathbf{F}_w = \rho \iint_S \left(\frac{\partial \Phi_w}{\partial t} \right) \mathbf{n}_j \cdot dS \tag{10.17}$$

$$\mathbf{F}_d = \rho \iint_S \left(\frac{\partial \Phi_d}{\partial t} \right) \mathbf{n}_j \cdot dS \tag{10.18}$$

$$\mathbf{F}_s = \rho \iint_S (gz) \mathbf{n}_j \cdot dS \tag{10.19}$$

Multibody hydrodynamics

Hydrodynamic loads, motion, and responses are significantly influenced by multibody hydrodynamic interactions. When a body oscillates, it radiates waves. Some of these radiated waves, which can be regarded as incident waves for the other bodies, interact with the neighboring body, resulting in diffraction phenomena. Other waves radiate to infinity, which would also be the case in a single-body model with no other body in close proximity.

To model this interaction between two bodies, a similar approach as described above is employed. For two bodies, each possessing six conventional rigid-body modes, the extended indices j = 7, 8, ..., 12 are used to define the wave force and moment components of the second body.

Wave spectrum

Linear wave theory can be applied to irregular waves and provide a statistical representation of ocean waves. An ocean wave with a random distribution can be described by its wave energy spectrum which specifies the energy distribution over a range of frequencies. The wave amplitude A_j can be calculated using this wave spectrum:

$$\frac{1}{2}A_j^2 = S_\eta(\omega_j)\Delta\omega \tag{10.20}$$

in which $\Delta\omega$ is the constant wave frequency step. The free surface elevation follows a Gaussian distribution for small amplitude irregular waves. The variance σ_η^2 of this distribution is equal to the area under the spectrum:

$$\sigma_\eta^2 = \int_0^\infty S_\eta(f)df \tag{10.21}$$

Ocean waves can be described by the wave spectrum under the assumption that the sea is a stationary random process. For analyses of marine operation the spectrum is assumed time-invariant for a period of 3 hours [42], although [51] mentions a period between 0.5 and 10 hours. This is also known as the short-term description of the sea.

Just as wave theories, there are several different empirical spectra and the frequency distribution of ocean waves differs per spectra. The Pierson-Moskowitz (PM) spectrum dates from 1964 and is only dependent on the peak frequency f_p. Here it is assumed that the sea state is fully developed and an equilibrium with the wind is achieved. The modified two-parameter PM spectrum [53] is also dependent on the significant wave height H_s, originally defined as the the mean height of the $\frac{1}{3}$ highest waves.

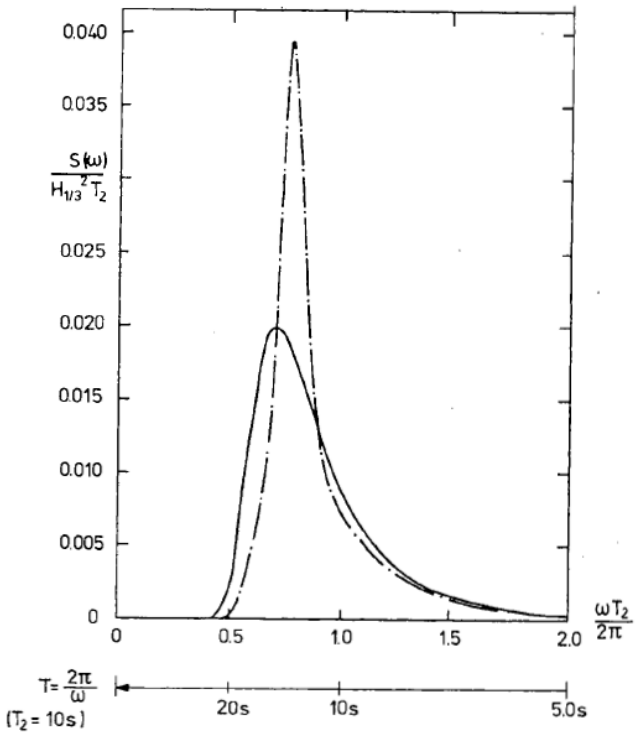

Figure 10.3: Comparison of modified PM (solid line) and JONSWAP (dotted line) wave spectrum [51]

In 1973 the Joint North Sea Wave Observation Project (JONSWAP) was created to describe storms of limited fetch, which indicates that the wave energy is limited by the size of the wave generation

area [43]. In practice sea states are seldom fully developed due to non-linear wave interactions. The peak enhancement factor γ was introduced to fit the measurements better and make the distribution more peaky. The factor is site-specific and for North-Sea sites usually $\gamma = 2 - 3$ is applied [53]. For a fully developed sea, which indicates that the waves are not fetch-limited, $\gamma = 1$ and the JONSWAP reduces to the PM spectrum. The modified PM and JONSWAP spectrum are compared in figure 10.3. The JONSWAP wave spectrum S_{JS} is defined as:

$$S_{\mathrm{JS}}(f) = 0.3125 \cdot H_{\mathrm{S}}^2 \cdot T_p \cdot \left(\frac{f}{f_{\mathrm{p}}}\right)^{-5} \cdot \exp\left(-1.25 \cdot \left(\frac{f}{f_{\mathrm{p}}}\right)^{-4}\right) \cdot (1 - 0.287 \cdot \ln\gamma) \cdot \gamma^{\exp\left(-0.5 \cdot \left(\frac{\frac{f}{f_{\mathrm{p}}} - 1}{\sigma}\right)^2\right)} \tag{10.22}$$

with

$$\gamma = \begin{cases} 5 & \text{for} \quad \frac{T_p}{\sqrt{H_s}} \leq 3.6 \\ \exp\left(5,75 - 1,15\frac{T_p}{\sqrt{H_s}}\right) & \text{for} \quad 3.6 \leq \frac{T_p}{\sqrt{H_s}} \leq 5 \\ 1 & \text{for} \quad \frac{T_p}{\sqrt{H_s}} > 5 \end{cases} \tag{10.23}$$

$$\begin{array}{lll} \sigma = 0.07 & \text{for} & f \leq f_{\mathrm{p}} \\ \sigma = 0.09 & \text{for} & f > f_{\mathrm{p}} \end{array} \tag{10.24}$$

In which the JONSWAP wave spectrum S_{JS} is dependent on the significant wave height (H_s), the peak period (T_p), the wave frequency (f), the peak wave frequency (f_p) and the peak enhancement factor (γ).

The chosen wave spectrum can thus be parametrized for the site-specific environmental parameters such as wave direction, significant wave height and wave period to decide whether their vessel can operate in such conditions.

Appendix B: Wave force RAO

Tri-floater wave force RAO

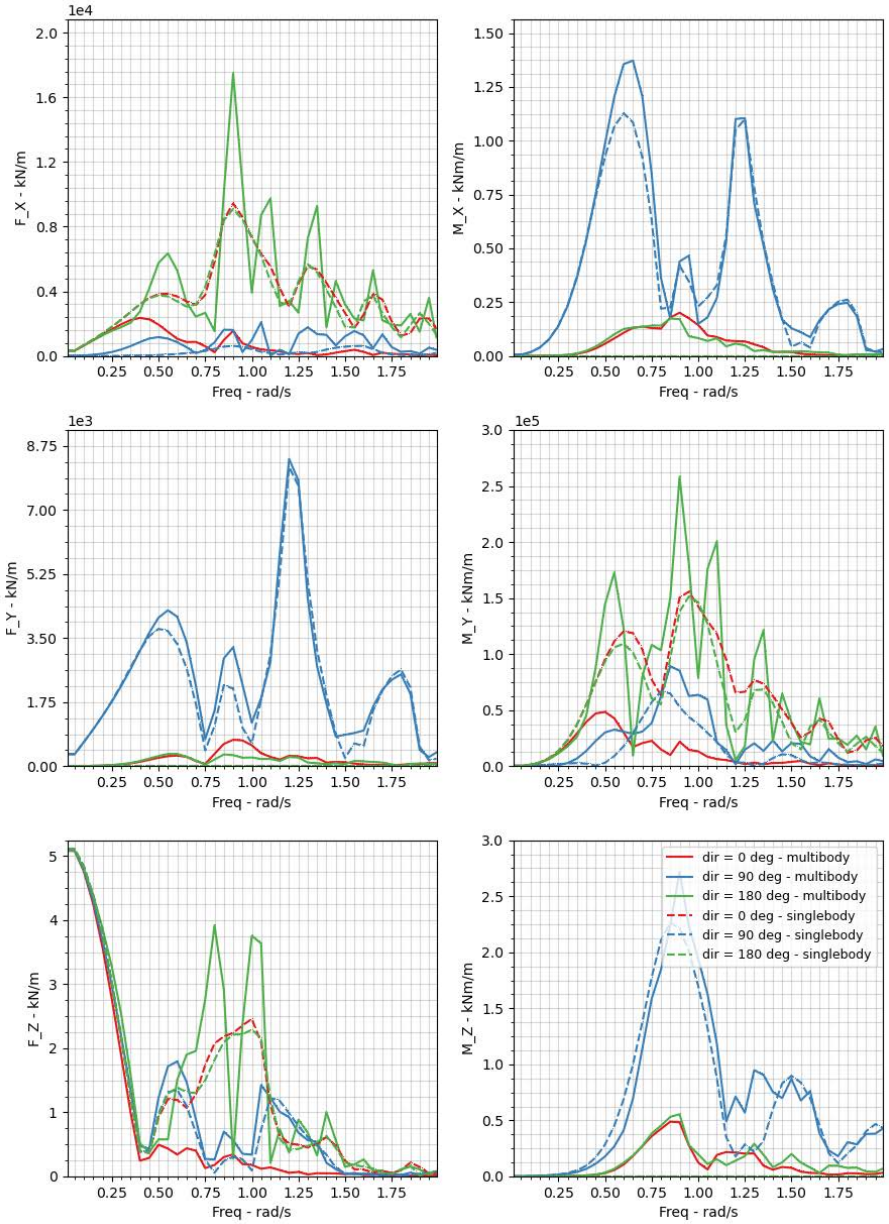

Figure 10.4: Tri-floater wave forces and moments in the single-body and multibody model for incoming waves at a wave angle of 0, 90 and 180 °.

Vessel wave force RAO

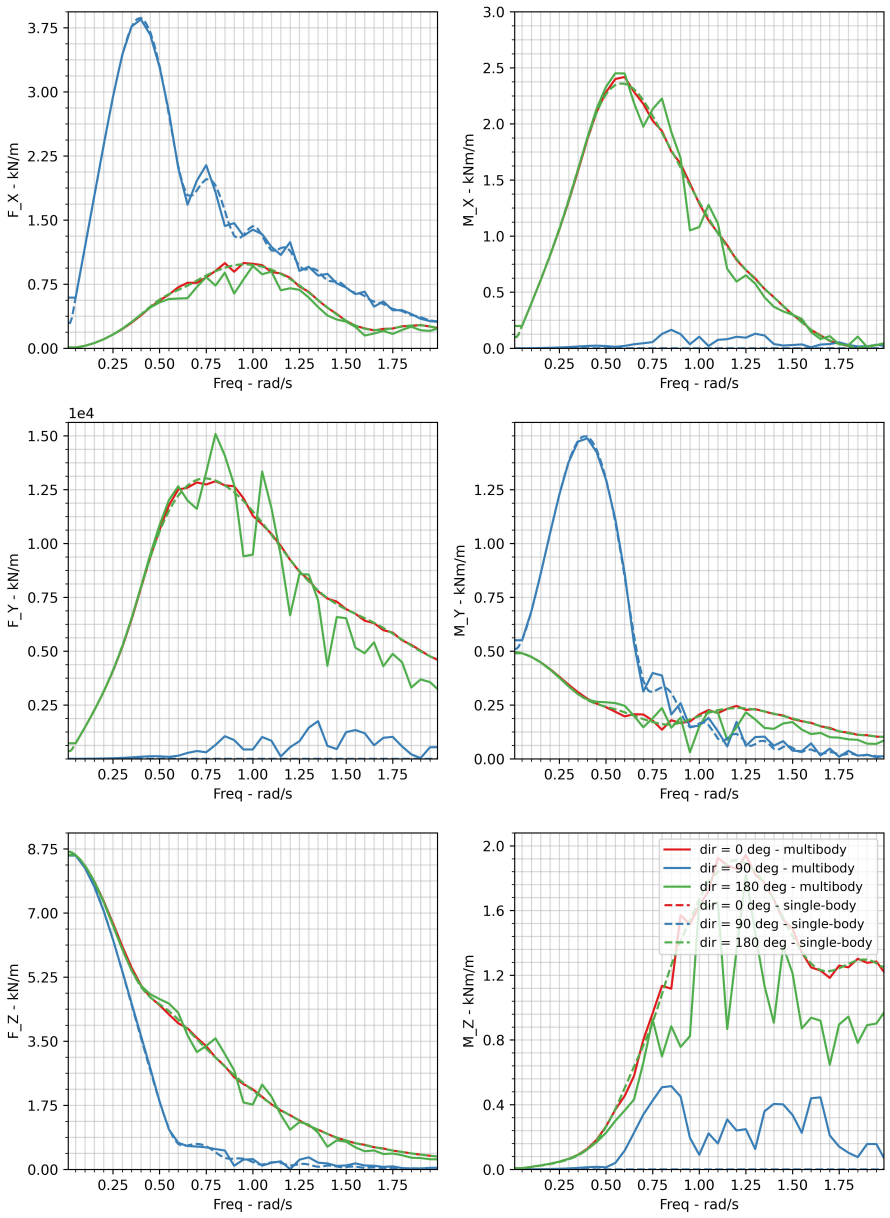

Figure 10.5: Vessel wave forces and moments in the single-body and multibody model for incoming waves at a wave angle of 0, 90 and 180 °.

Appendix C: Relative phase

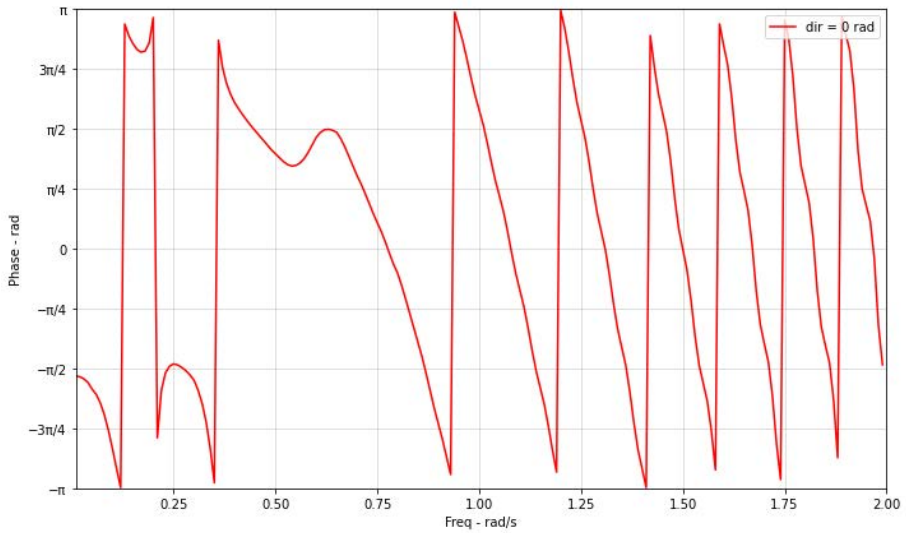

Figure 10.6: Relative phase at a wave angle of 0 °.